Biogeosciences Discuss., doi:10.5194/bg-2017-119, 2017
Manuscript under review for journal Biogeosciences
Discussion started: 13 April 2017

Carbon mineralization in Laptev and East Siberian Sea shelf and slope sediment

Volker Brüchert[1,3], Lisa Bröder[2,3], Joanna E. Sawicka[1,3], Tommaso Tesi[2,3,5], Samantha P. Joye[6], Xiaole Sun[4,5], Igor P. Semiletov[7,8,9], Vladimir A. Samarkin[6]

[1] Department of Geological Sciences, Stockholm University, Stockholm, Sweden
[2] Department of Environmental Sciences and Analytical Chemistry, Stockholm University, Stockholm, Sweden
[3] Bolin Centre for Climate Research, Stockholm University, Stockholm, Sweden
[4] Baltic Sea Research Center, Stockholm University, Stockholm, Sweden
[5] Institute of Marine Sciences – National Research Council, Bologna, Italy
[6] Department of Marine Sciences, University of Georgia, Athens, U.S.A.
[7] International Arctic Research Center, University Alaska Fairbanks, Fairbanks, USA
[8] Pacific Oceanological Institute, Russian Academy of Sciences, Vladivostok, Russia
[9] Tomsk National Research Politechnical University, Tomsk, Russia

Abstract The Siberian Arctic Sea shelf and slope is a key region for the degradation of terrestrial organic material transported from the organic carbon-rich permafrost regions of Siberia. We report on sediment carbon mineralization rates based on O_2 microelectrode profiling, intact sediment core incubations, ^{35}S-sulfate tracer experiments, porewater dissolved inorganic carbon (DIC), $\delta^{13}C_{DIC}$, and iron, manganese, and ammonium concentrations from 20 shelf and slope stations. This data set provides a spatial overview of sediment carbon mineralization rates and pathways over large parts of the outer Laptev and East Siberian Arctic shelf and slope, and allowed us to assess degradation rates and efficiency of carbon burial in these sediments. Rates of oxygen uptake and iron and manganese reduction were comparable to temperate shelf and slope environments, but bacterial sulfate reduction rates were comparatively low. In the topmost 20 to 50 cm of sediment, aerobic carbon mineralization dominated degradation and comprised on average 82% of the depth-integrated carbon mineralization. Oxygen uptake rates and ^{35}S-sulfate reduction rates were higher in the eastern East Siberian Sea shelf compared to the Laptev Sea shelf. DIC/NH_4^+ ratios in porewaters and the stable carbon isotope composition of remineralized DIC indicated that the degraded organic matter on the Siberian shelf and slope was a mixture of marine and

Biogeosciences Discuss., doi:10.5194/bg-2017-119, 2017
Manuscript under review for journal Biogeosciences
Discussion started: 13 April 2017

terrestrial organic matter. Based on dual end member calculations, the terrestrial organic carbon contribution varied between 32% and 36%, with a higher contribution in the Laptev Sea than in the East Siberian Sea. Extrapolation of the measured degradation rates using isotope end member apportionment over the outer shelf of the Laptev and East Siberian Sea suggests that about 16 Tg C per year are respired in the outer shelf sea floor sediment. Of the organic matter buried below the oxygen penetration depth, between 0.6 and 1.3 Tg C per year are degraded by anaerobic processes, with a terrestrial organic carbon contribution ranging between 0.3 and 0.5 Tg per year.

Key words: Carbon mineralization, Arctic shelf and slope sediment, Laptev Sea, East Siberian Sea

1. Introduction

The biogeochemical fate of terrestrial organic carbon deposited on the Arctic shelf and slope is one of the most important open questions for the marine Arctic carbon cycle (e.g., Tesi et al., 2014; Macdonald et al., 2015; McGuire et al., 2009; Vonk et al, 2012). The total pan-Arctic terrestrial permafrost carbon reservoir has been estimated at about 1100 – 1500 Pg (Hugelius et al, 2014) – a carbon pool large enough to substantially affect the global atmospheric carbon dioxide pool over the next 100 years, even when only partially decomposed after thawing and oxidation (Schuur et al. 2015; Koven et al., 2015). Yet, there remains considerable uncertainty regarding the mineralization of terrestrial organic matter exported by rivers and coastal erosion to the Siberian shelf and slope (Tesi et al., 2014; Karlsson et al. 2015; Semiletov et al., 2011; Salvado et al., 2016).

Terrestrial organic matter transported to the Siberian shelf is of variable size, age, and molecular composition, which results in a range of qualitatively different carbon degradation rates of bulk carbon and individual molecular components. Size class analysis of the organic matter suggests that coarse organic material settles preferentially in near-shore environments, whereas finer organic fractions disperse offshore in repeated deposition-resuspension cycles gradually losing particular molecular components and overall reactivity (Wegner et al., 2013; Tesi et al., 2014, 2016). Substantial oxic degradation of organic matter may occur during near-bottom transport in resuspension-deposition cycles across the shelf (Bröder et al., 2016a). Up to 90% of certain biomarker classes may decompose during transport, whereby

Biogeosciences Discuss., doi:10.5194/bg-2017-119, 2017
Manuscript under review for journal Biogeosciences
Discussion started: 13 April 2017

most of the degradation may take place while the transported organic material resides in the sediment before being resuspended (Bröder et al., 2016a). However, without making approximations on transport direction, particle travel time and travel distance these studies cannot provide direct insights into the rates of carbon degradation and resultant CO_2 fluxes from sediment. By contrast, direct kinetic constraints provided by sediment carbon degradation rates can provide testable data for coupled hydrodynamic biogeochemical models that help assess the fate of land-exported terrestrial carbon pool on the Siberian shelf.

Relatively few studies have directly measured rates of carbon mineralization rates in Siberian shelf sediment (e.g., Boetius and Damm, 1998; Grebmeier et al., 2006; Karlsson et al., 2015, Savvichev et al., 2007). Boetius and Damm (1998) used high-resolution oxygen microelectrode data to determine the surface oxygen concentration gradients and oxygen penetration depths in a large number of sediment cores from the shelf and slope of the Laptev Sea. Based on corresponding sediment trap and export productivity data, they concluded that the annual marine organic carbon export in the Laptev Sea shelf and slope was sufficiently high to explain the observed oxygen uptake rates. Current understanding therefore holds that due to the long annual ice cover and low productivity on the eastern Siberian Arctic shelf and slope, only a small amount of marine organic carbon is exported and buried in Laptev and East Siberian Sea shelf sediment. The highly reactive fraction of fresh organic matter is thought to degrade in the surface sediment (Boetius and Damm, 1998). Consequently, anaerobic respiration in buried sediment has been thought to be negligible and to reflect the degradation of unreactive terrestrially derived carbon compounds. To our knowledge, with the exception of a recent study by Karlsson et al (2015) a more direct assessment of terrestrial carbon-derived mineralization rates in buried shelf and slope sediment has not been reported for the East Siberian Arctic Sea.

In this study, we present data from oxygen microelectrode profiling experiments, porewater data of dissolved inorganic carbon and its stable carbon isotope composition, and ^{35}S-sulfate reduction rate experiments along a shelf-slope transect near 125°E in the Laptev Sea. Samples were taken during the summer 2014 on the SWERUS-C3 expedition with the Swedish icebreaker Oden. We combined these data with porewater analysis of dissolved ammonium, sulfate, iron, and manganese to assess the major carbon degradation pathways and rates across the extensive outer Laptev and Siberian shelf and slope.

Biogeosciences Discuss., doi:10.5194/bg-2017-119, 2017
Manuscript under review for journal Biogeosciences
Discussion started: 13 April 2017

2. Materials and methods

2.1. Sample collection

Samples were collected at 20 stations from 40 to 3146 m water depth in the western Laptev and East Siberian Sea (Fig. 1 and Table 1). In this study we only report on sampling sites that showed no methane gas plumes, acoustic anomalies in the water column, or sediment blankings indicative of rising gas. In areas of active ebullition from the seafloor as seen by video imagery and acoustic gas blankings in the water column, the biogeochemistry of sea floor processes such as bacterial sulfate reduction, DIC concentration and its carbon isotope composition, and oxygen uptake are affected by methane oxidation. These methane cycling-related signals overprint the biogeochemistry imparted by carbon mineralization and are reported in a separate study.

Sediment stations had variable ice cover (Table 1). In the Laptev Sea, except for the deep-water slope stations between 3146 m and 2106m, all stations had open water. By contrast, ice cover exceeded 75% in the East Siberian Sea to the west and east of Bennett island (Station 40 to 63). Sediments with well-preserved sediment surfaces were collected with a Multicorer (Oktopus GmbH, Kiel, Germany) that simultaneously takes 8 sediment cores over an area of about 0.36 m^2 with acrylic tubes (9.5 cm diameter, 60 cm length) to 40 cm depth preserving clear water on top of the sediment. At stations 6, 23, and 24 an underwater video system (Group B Distribution Inc., Jensen Beach, U.S.A.) was mounted on the multicore frame to record the deployment and recovery, and to document the sea floor habitat. For the investigations all cores were taken from the same cast. Two of the cores were used to determine ^{35}S-sulfate reduction rates and porosity. In addition, one core with predrilled 3.8 mm holes sealed with electric tape was used to extract porewaters with rhizons (Rhizosphere Research Products BV, Wageningen, Netherlands). A fifth core was used for microelectrode measurements of dissolved oxygen concentration profiling, and finally, four other cores were used for whole-core incubations to determine benthic fluxes of dissolved oxygen, dissolved inorganic carbon, and nutrients. The cores were capped with rubber stoppers until further subsampling usually within 30 minutes. For sulfate reduction rates, the cores were subsampled with 40 or 50 cm long acrylic tubes (26 mm inner diameter) prepared with silicon-sealed holes, drilled at distances of 1 cm. For whole-core incubations, the cores were sub-sampled with 25 cm-long, 60 mm-wide tubes (56 mm id) to 12 cm depth. Likewise, a 60 mm diameter tube (56 mm id) was collected for microelectrode measurements preserving

Biogeosciences Discuss., doi:10.5194/bg-2017-119, 2017
Manuscript under review for journal Biogeosciences
Discussion started: 13 April 2017

about 3 cm of the overlying bottom water. For intact whole-core incubations, temperature-controlled aquaria were filled with bottom water that was collected from a CTD rosette from the same station by collecting water from four ten-liter rosette bottles usually ~5 meters above the sea floor. All sediment cores were closed with a stopper retaining the water on top of the sediment and stored at 1.5°C in an incubator until further processing.

2.2. Microelectrode oxygen profiles

High-resolution O_2-profiles across the water-sediment interface were obtained to determine oxygen penetration depths and diffusive oxygen uptake (Rasmussen and Jørgensen, 1992; Glud, 2008). The 60 mm tubes were placed in an aquarium filled with bottom water from the same station, overflowing the sediment core. The water temperature was kept to ~1°C by a cooling unit (Julabo GmbH, Seelbach, Germany). In exceptional cases when there was not sufficient bottom water available to fill the aquarium, bottom water was used from a pump system. A stable diffusive boundary layer above the sediment was created by passing air from an aquarium pump over the water surface with a Pasteur pipette creating a slow rotational motion of water inside the core. At each station six to eight O_2 microprofiles were measured using Clark-type oxygen microelectrodes (OX-50, Unisense, Århus Denmark) mounted on a motor-driven micromanipulator (MM33, Unisense, Århus Denmark). O_2 sensors were calibrated with fully oxygenated bottom water from the same station at ~1°C for saturation and for anoxic conditions by dissolving Na_2SO_3 dissolved in the same water. The first profile in each core was measured with a resolution of 1000µm as a quick scan to locate the sediment surface and to adjust the measuring range. Then the vertical resolution was increased to 100-500µm and additional five to seven profiles were measured at different points on the surface, approximately one cm apart from each other.

2.3. Whole-core sediment incubations

Four intact cores with undisturbed sediment surfaces and clear overlying water were subsampled in the laboratory in acrylic tubes (i.d. 56 mm, height 25 cm) retaining about 10 cm of the overlying water. The sediment and water height in the tubes were approximately 10 cm. The cores were incubated in a 40-liter incubation tank filled with bottom water from the same station. Before the incubation the overlying water in the cores was equilibrated with

Biogeosciences Discuss., doi:10.5194/bg-2017-119, 2017
Manuscript under review for journal Biogeosciences
Discussion started: 13 April 2017

bottom water in the tank. The overlying water in the cores was stirred by small magnetic bars mounted in the core liners and driven by an external magnet at 60 rpm. The cores were pre-incubated uncapped for 6 hours and subsequently capped and incubated for a period of 6 to 24 hours depending on the initial oxygen concentration in the bottom water. 2D oxygen sensor spots (Firesting oxygen optode, PyroScience GmbH, Aachen, Germany) with a sensing surface of a diameter of 5 mm were attached to the inner wall of two incubation cores. The sensor spots were calibrated against O_2-saturated bottom water and oxygen-free water following the manufacturer's guidelines accounting for temperature and salinity of the incubation water. Measurements were performed with a fiberoptic cable connected to the spot adapter fixed at the outer core liner wall at the spot position. The O_2 concentration was continuously logged during incubations. Sediment total oxygen uptake (TOU) rates were computed by linear regression of the O_2 concentration over time. 5 ml of overlying water were removed over the course of the incubation used for nutrient and dissolved CO_2 analysis as described below. Linear regression best fits were used to determine the exchange fluxes of dissolved CO_2 and ammonium.

2.4. Extracted porewater analysis

Porewater samples for concentration measurements of total dissolved CO_2 (DIC), sulfate and ammonium were obtained using the methods described in Seeberg-Elverfeldt et al. (2005). Rhizons were treated for 2 hours in 10% HCl solution, followed by two rinses with deionized water for 2 hours and final storage in deionized water. The rhizons were connected to 10 mL disposable plastic syringes with inert pistons (VWR, Stockholm, Sweden) via polyethylene 3-way luer-type stopcocks (Cole-Parmer, U.S.A.) and inserted in 1 cm intervals through tight-fitting, pre-drilled holes in the liner of the sediment cores. The first mL of pore water was discarded from the syringe. No more than 5 ml were collected from each core to prevent cross-contamination of adjacent porewater due to the suction effect (Seeberg-Elverfeldt et al., 2005). The collected porewater was divided into four different aliquots for later chemical analysis. For dissolved sulfate analysis, 1 ml of porewater was preserved with 200 µl of 5% zinc acetate solution and frozen. For ICP-AES analysis of dissolved metals and major cations, 1 ml of porewater was preserved with 100 µl of 10% Suprapur HNO_3 and stored cold. For analysis of dissolved ammonium, 2 ml of porewater were frozen untreated. For analysis of dissolved inorganic carbon, 2 ml of porewater were preserved with 100 µl

Biogeosciences Discuss., doi:10.5194/bg-2017-119, 2017
Manuscript under review for journal Biogeosciences
Discussion started: 13 April 2017

191 10% $HgCl_2$ and stored cold in brown glass vials without headspace. Sulfate concentration was
192 measured on diluted aliquots on a Dionex System IC 20 ion chromatograph. DIC
193 concentrations were determined by flow injection analysis (Hall and Aller, 1992). Ammonium
194 was determined on a QUAATRO 4-channel flow injection analyzer (Seal Analytical).
195 Dissolved iron and manganese were determined on diluted aliquots by ICP-AES (Varian
196 Vista AX). For carbon isotope analysis of dissolved inorganic carbon, 1 ml of porewater was
197 filled into 12 ml exetainers to which 1 ml of concentrated phosphoric acid was added. The
198 carbon isotope composition of the formed CO_2 was analyzed on a GasbenchII-MAT 253
199 isotope ratio mass spectrometer coupled to a GC-PAL autosampler. Results are reported in the
200 conventional delta notation relative to PDB. Precision of isotope analysis is 0.1‰.
201
202 **2.5. Reaction transport modelling**

203 Reaction rates and fluxes were estimated from the concentration profiles of dissolved
204 oxygen, manganese, iron, and dissolved inorganic carbon according to the general reaction-
205 transport equation accounting for diffusion and advection exemplified here for dissolved
206 oxygen according to

207 $$\frac{dO_2}{dt} = \frac{\partial D_s \frac{\partial O_2}{\partial z}}{\partial z} + \frac{\partial v O_2}{\partial z} + \omega \frac{\partial O_2}{\partial z} + \sum R \qquad (1)$$

208 At steady state, the rate of the concentration change reflects the balance between the
209 consumption due to respiration and oxidation of reduced inorganic compounds (R) against
210 diffusion and advection due to bioirrigation into sediment (Glud, 2008). D_s is the sediment
211 diffusion coefficient and was calculated for the experimental temperature and salinity
212 according to Boudreau (1997). The sediment diffusion coefficient D_s was recalculated from
213 the molecular diffusion coefficient D_o according to $D_s = D_o / \theta^2$, where $\theta^2 = 1 - \ln(\varphi^2)$, where
214 φ is porosity and θ is tortuosity (Boudreau, 1997). Sediment burial ω was based on ^{210}Pb-
215 based sediment accumulation rates (Bröder et al., 2016b). The advection rate υ was estimated
216 by stepwise optimization by fitting an oxygen concentration profile to the measured
217 concentration data using the least square fitting procedure of the program Profile (Berg et al.,
218 1998).
219

Biogeosciences Discuss., doi:10.5194/bg-2017-119, 2017
Manuscript under review for journal Biogeosciences
Discussion started: 13 April 2017

220 **2.6. ^{35}S-Sulfate reduction rates**

221 Bacterial sulfate reduction rates (^{35}S-SRR) sediment cores were subsampled in 40-cm
222 long 28 mm-diameter cores with 1-cm spaced, silicon-sealed, pre-drilled small holes on the
223 side for injections. For the incubation, the whole-core incubation method by Jørgensen (1978)
224 was used. $^{35}SO_4^{2-}$ tracer solution was diluted in a 6 ‰ NaCl solution containing 0.5 mM SO_4^{2-}
225 and 2.5 µl of the tracer solution (200kBq) was injected through the pre-drilled holes. The
226 cores were then capped and sealed in plastic wrap foil and incubated for 8 hours at the
227 respective bottom water temperatures. After this time, the incubations were stopped by
228 sectioning the core in 1-cm intervals to 5 cm depth and in two centimeter intervals below this
229 depth to the bottom of the core. Sediment sections were transferred into 50 ml plastic
230 centrifuge tubes containing 20 ml zinc acetate (20% v/v) and shaken vigorously and frozen.
231 The total amount of ^{35}S-labeled reduced inorganic sulfur (TRS) was determined using the
232 single-step cold chromium distillation method by Kallmeyer et al. (2004). TRS and
233 supernatant sulfate were counted on a TriCarb 2095 Perkin Elmer scintillation counter. The
234 sulfate reduction rate was calculated using the following equation (Jørgensen, 1978):

235 $$^{35}SRR = \left(TRI^{35}S \times 1.045 \Big/ (^{35}SO_4^{2-} + TRI^{35}S) \right) \times [SO_4^{2-}]/\rho T \qquad (2)$$

236 where $[SO_4^{2-}]$ is the pore water sulfate concentration corrected for porosity ρ, TRI^{35}S and
237 $^{35}SO_4^{2-}$ are the measured counts (cpm) of sulfate and total reduced inorganic sulfur species,
238 respectively, 1.045 is a correction factor accounting for the kinetic isotope effect of ^{35}S
239 relative to ^{32}S, and T is the incubation time. The sulfate reduction rate is reported as nmol cm^{-3} day^{-1}. ^{35}SRR were measured in two parallel cores for all depth intervals. The incubation
241 experiments were conducted between July 15 and August 20, but for logistical reasons
242 (transport to Stockholm) the distillation of the samples was conducted between December 10,
243 2014 and April 2, 2015 so that between 1.7 and 2.7 half-lives of ^{35}S (87.4 days) had passed
244 before all samples were processed. The resulting detection limit of the rate measurements
245 accounting for distillation blanks and radioactive decay of ^{35}S between experiment and
246 laboratory workup was 0.01 nmol cm^{-3} day^{-1}.

247

248

Biogeosciences Discuss., doi:10.5194/bg-2017-119, 2017
Manuscript under review for journal Biogeosciences
Discussion started: 13 April 2017

3. Results

3.1. Physical and chemical bottom water conditions

Table 1 summarizes the general site characteristics of the investigated sediment stations. Bottom water salinity varied between 34.9 ‰ in the outer Laptev Sea at 3146 m depth (Station 1) to 29.1 ‰ in the East Siberian Sea at 40 m (Station 45). The lower salinity in the East Siberian Sea can be attributed to longshore transport of freshwater eastward from the Lena River. Bottom water temperatures varied between -1.8°C at Station 27 and 0°C at Station 37, but there was no regional trend in the data. Cored sediment consisted of silty clays to clayey silts. Slope sediment had a distinctly chocolate brown color throughout the cored interval, whereas shelf sediment only had a 1 to 4 cm-thick chocolate-brown interval, below which the sediment color changed to olive gray and greenish gray. In the eastern part of the East Siberian Sea, the sediment was mottled black-olive below 10 cm depth. Iron-manganese concretions were found between 2 cm and 10 cm depth at stations 24, 42, and 43, but were also observed at other stations on the shelf that were not part of this study. Generally, few benthic macrofauna was present and bioturbation was weak or absent. Benthic macrofauna, when present, consisted mainly of brittle stars, isopods, few polychaetes, and rare bivalves. All bottom waters were well-oxygenated with concentrations higher than 190 µmol/l, but the shelf bottom-waters in the East Siberian Sea had generally lower concentrations than in the Laptev Sea and bottom waters on the continental slope had lower oxygen concentrations than on the shelf. Concentrations of bottom-water ammonium ranged between 0.2 µmol/L and 1.8 µmol/L. Generally, the slope stations and the shelf stations nearest to the Lena delta had the highest ammonium concentrations, whereas the other shelf stations showed no clear regional trend other than proximity to the Lena delta. Bottom water dissolved inorganic carbon concentrations varied between 2086 µM (Station 53) and 2598 µM (Station 27), and the stable carbon isotope composition of DIC in the waters overlying the cores were between -0.5 ‰ and -6.5 ‰ vs. VPDB.

3.2. Dissolved oxygen, manganese, and iron

We show representative profiles of oxygen concentrations in Figure 2 for the Laptev Sea slope station 1, the Laptev Sea shelf stations 23, 30, 45, and the East Siberian Shelf Sea 53 and 63. Oxygen penetration depths varied between 3 mm at Station 58 and more than 60

Biogeosciences Discuss., doi:10.5194/bg-2017-119, 2017
Manuscript under review for journal Biogeosciences
Discussion started: 13 April 2017

mm in all slope sediments (Table 2). For the Laptev Sea slope stations 1, 2, 3, and 4, the maximum depth of oxygen penetration could not be determined, because at penetration greater than 60 mm the conical sensor needle opened a hole in the sediment through which oxygen-containing bottom water could potentially have entered the sediment at depth thereby artificially extending the oxygen penetration depth. In the slope-to-shelf transects the oxygen penetration depth decreased from >60 mm off-shore to 10 mm at the most inshore station in the Laptev Sea and the East Siberian Sea. At the two easternmost shelf stations 58 and 63, we measured the lowest oxygen penetrations depths, 3 mm and 4 mm, respectively. Evidence for bioturbation and bioirrigation based on multiple microelectrode profile measurements per core was rare. Only at Station 48 a clear increase in oxygen concentrations below the sediment surface was observed, indicative of active bioirrigating macrofauna. However, even at this station, based on investigations in parallel multicore casts, fauna was not abundant. At all other stations, oxygen concentrations decreased exponentially with depth. Fitting of the oxygen concentration profiles to the steady advection-diffusion-transport model (Eq. 1) yielded fluxes that varied between 0.81 and 11.49 mmol m^{-2} d^{-1} (Table 2). These calculated O_2 fluxes compared well with total oxygen uptake rates calculated from whole-core incubations using 2D optode sensor spots (Table 3). The good fit between the two methods also supports the notion that bioirrigation and bioturbation effects from meiofauna and macrofauna were minor.

In the slope sediment at Station 1, concentrations of dissolved manganese and iron were low throughout the cored depth interval and below 0.2 and 0.5 µM, respectively. The exception was a small increase for both elements between 4 and 8 cm depth and 14 and 20 cm depth to concentrations of less than 3 µM, possibly due to slightly more degradable organic material in these depth intervals (Fig. 2). A similar concentration profile was found for the other slope station 4 (data not shown), but here concentrations were below 2 µM throughout for both dissolved iron and manganese and only slightly higher in the topmost cm. On the shelf, in the Laptev Sea (Station 23 and 30), concentrations of dissolved manganese and iron were below 0.3 µM and 1.5 µM, respectively, in the top 2 cm and 3 cm at Station 23, before increasing to maximum concentrations of 69 and 134 µM. At both stations, metal concentrations decreased again below the concentration maximum indicating that deeper buried sediment was not a source of the metals and that the dominant source of iron and manganese was reduction in the topmost 5 cm of sediment. There was a general trend of increasing manganese concentrations from west to the east. At Station 30 in the Laptev Sea,

Biogeosciences Discuss., doi:10.5194/bg-2017-119, 2017
Manuscript under review for journal Biogeosciences
Discussion started: 13 April 2017

the concentration of dissolved manganese was less than 0.3 µM in the topmost cm, but increased steeply before increasing to maximum concentrations of 189 µM at 9 cm depth. Similarly, dissolved iron concentrations were below 1 µM to 4 cm depth and then increased to 144 µM. Again, below the maximum, both iron and manganese porewater concentrations decreased with increasing sediment depth. Even higher iron and manganese concentrations were found in the East Siberian Sea (Stations 45, 53, 63), where dissolved manganese already increased from the bottom water to concentrations of 20 µM in the topmost centimeter of sediment, and iron increased to above 1 µM below 2 cm depth. The steepest manganese concentration gradient was found at Station 63 in the easternmost East Siberian Sea, where concentrations were 501 µM in the first cm of sediment with a concentration maximum of 548 µM at 2.5 cm depth and decreasing below this depth to 115 µM at 30 cm depth. Station 63 differed with respect to dissolved iron concentrations from the other stations, because here dissolved iron showed two small peaks at 3.5 cm and 7 cm, and concentration increased substantially only below 17 cm depth to concentrations of 189 µM.

3.3. ^{35}S-Sulfate reduction rates and sulfate

Sulfate concentrations showed minor depth gradients at all sampling sites (Fig. 3) and decreased from starting concentrations between 23.9 mM and 28.1 mM by 0.4 mM to 2.5 mM from the top to the bottom of the cores. At all stations, turnover of ^{35}S-tracer was recorded from the topmost sediment interval to the bottom of the core indicating active bacterial sulfate reduction (Fig. 3). Depth-integrated rates over the recovered core lengths varied between 0.03 and 1.41 mmol m^{-2} d^{-1} (Table 2). The integrated rates were lowest at Station 1 at 3146 m in the Laptev Sea and highest at the Station 63 in the easternmost East Siberian Sea. Across the shelf, depth-integrated rates increased from the west to the east. Example depth profiles of depth-specific sulfate reduction rates are shown in Fig. 3 for the same six stations as previously. At Station 1, these rates ranged from 0.03 to 0.38 nmol cm^{-3} d^{-1}. At this station, the variability between replicate cores was large, which is attributed to the fact that many rates were near the detection limit in our handling procedure. Overall, sulfate reduction was higher in the top 10 cm of sediment, but showed no pronounced change with depth at this station. This suggests that the reactivity of the organic material did not change substantially over the cored depth interval. The second slope station, Station 4, showed a similar rate-depth profile than Station 1. Depth profiles for the mid-outer shelf stations 23 to 63 all showed

Biogeosciences Discuss., doi:10.5194/bg-2017-119, 2017
Manuscript under review for journal Biogeosciences
Discussion started: 13 April 2017

broad sub-surface maxima between 2.5 and 17.5 cm, but the depths of the rate maxima differed between the different stations (Fig. 3). Peak rates varied between 0.6 nmol cm^{-3} d^{-1} at Station 30 and 39 nmol cm^{-3} d^{-1} at Station 63. The second highest rate, 7.6 nmol cm^{-3} d^{-1}, was found at the station nearest to the Lena delta, Station 23. At all stations, sulfate reduction rates decreased from the maxima to rates below 1 nmol cm^{-3} d^{-1} or to below the detection limit at the bottom of the cores. A particularly sharp decrease in the sulfate reduction rate was observed between 8 and 9 cm at Station 63, where rates dropped from 8.5 to 0.1 nmol cm^{-3} day^{-1} over 1 cm depth. Since sulfate was abundant throughout the cored intervals, this order-of-magnitude decrease indicates substantial changes in the reactivity of buried organic matter. Although no abrupt change in grain size or organic carbon was observed in this core, it is likely that a historical change in organic sedimentation had taken place during deposition across this time interval.

3.4. Porewater dissolved inorganic carbon (DIC), ammonium (NH_4^+), and $\delta^{13}C_{DIC}$

Porewater concentrations of dissolved inorganic carbon (DIC) and ammonium (NH_4^+) increased with depth at all stations (Fig. 4). The decrease of DIC was between 0.6 mM (Station 23) and 7.2 mM (Station 50) over the cored sediment depths and ammonium concentrations increased between 16.8 µM (Station 1) and 549 µM (Station 50). The steepness of the depth gradients was consistent with the rates of oxygen uptake and bacterial sulfate reduction for the different stations. The porewater pattern at Station 63 is an exception, because this station had the highest oxygen uptake and the highest sulfate reduction rates of all stations, but showed only a modest increase in DIC and NH_4^+ concentrations by 1.5 mM and 57 µM, respectively, over the cored sediment depth. This apparent discrepancy can be explained by the very low rates of sulfate reduction and sedimentation below 10 cm depth. Since these deeper layers have not produced large amounts of DIC and NH_4^+, only the surface 10 cm contribute significantly to total carbon mineralization and ammonium production.

DIC/NH_4^+ ratios of remineralized inorganic carbon and NH_4^+ were corrected for the bottom water DIC and NH_4^+ concentrations. For the anoxic parts of the sediment, DIC/NH_4^+ ratios varied between 9.8 for Station 24 and 65 for Station 1, with an overall mean DIC/NH_4 ratio of 13.4. The $\delta^{13}C$ values of DIC consistently decreased with sediment depth indicating the addition of ^{13}C-depleted remineralized carbon to DIC. The greatest downcore depletion in ^{13}C

376 was observed at Stations 45, 48, and 50, where $\delta^{13}C$ of DIC decreased from -2.0 ‰ near the
377 sediment surface to -13.9, -16.4, and -18.6 ‰ at the bottom of the cores (Fig. 4).

378

379 **4. Discussion**

380 **4.1. Modelled oxygen, iron, and manganese reduction rates**

381 Results of the reaction transport modelling of dissolved oxygen, iron, and manganese
382 concentration profiles for Station 23 are shown in Fig. 5. O_2 consumption rates exceeded
383 sulfate, iron, and manganese reduction rates by a factor of more than 100 (Fig. 5). For the
384 shelf stations, most of the carbon oxidation therefore takes place in the topmost 5 mm. The
385 reaction rate profiles for iron and manganese reduction indicate that manganese reduction
386 dominates in the topmost 2 cm of sediment followed by co-existing iron and sulfate reduction
387 below (Fig. 5). These observations are consistent with results from the northern Barents Sea
388 by Vandieken et al. (2006) and Nickel et al. (2008). Optimal fits of the concentration profiles
389 required a sediment mixing coefficient of 1 x 10^{-4} cm^2 sec^{-1} in the topmost 2 cm of sediment
390 at Stations 23 and 53. For the other stations, optimal fits required no sediment mixing by
391 bioturbation or advective porewater transport by bioirrigation. This result is consistent with
392 the modelling results of the oxygen microelectrode profiles and the low numbers of
393 bioturbating macrofauna in the outer shelf sediment. Bacterial sulfate reduction was detected
394 already at a depth where the sediment was still brown indicating abundant iron
395 oxyhydroxides. It is therefore likely that the modelled negative iron production rates at the
396 sediment surface indicate iron oxidation in the mixed upper layer. This pattern was not
397 observed for manganese, which is consistent with incomplete manganese oxidation at the
398 sediment surface and loss of dissolved manganese to the bottom water. The latter observation
399 supports the assessment by Macdonald and Gobeil (2012) that Arctic shelves can export
400 dissolved manganese to the Arctic interior. Coexistence of net iron reduction and sulfate
401 reduction at the same depths make it difficult to quantify how much of the iron reduction is
402 coupled to heterotrophic carbon oxidation and to the re-oxidation of sulfide produced from
403 bacterial sulfate reduction. Qualitatively, the presence of dissolved iron throughout the
404 measured porewater profile implies that iron reduction exceeded concomitant sulfate
405 reduction, iron sulfide precipitation, and reoxidation reactions, which supports the assessment
406 of net heterotrophic iron reduction. However, previous investigations of the importance of
407 iron and manganese reduction in Arctic shelf sediments have emphasized the importance of

Biogeosciences Discuss., doi:10.5194/bg-2017-119, 2017
Manuscript under review for journal Biogeosciences
Discussion started: 13 April 2017

directly coupled redox processes between iron and manganese (. It is also important to note that iron and manganese oxyhydroxides can sorb Mn^{2+} and Fe^{2+} (Canfield et al. 1993). The concentrations of dissolved Fe^{2+} and Mn^{2+} may therefore underestimate the actual concentrations of the reduced forms in these sediments.

Depth-integration of the modelled iron and manganese reduction rates and recalculation of the depth-integrated rates into carbon mineralization equivalents were performed and the respective carbon oxidation equivalents for these electron acceptors were calculated using an idealized $(CH_2O)_x$ stoichiometry for organic matter (Vandieken et al., 2006; Nickel et al., 2008). These rates were then used to calculate the contribution of the different aerobic and anaerobic electron acceptors to total carbon mineralization for 5 stations on the Laptev and East Siberian Sea shelf (Table 3). Accepting the simplifications and limitations of porewater-based rate calculations mentioned above, manganese and iron reduction contributed between 2.3 and 23.7% to the total anaerobic carbon mineralization and between 0.3 and 2.3% to the total carbon mineralization. Although these numbers may somewhat underestimate the contribution of metals to carbon mineralization as discussed above, our results suggest that bacterial sulfate reduction is by far the major anaerobic carbon mineralization pathway. This conclusion is consistent with the assessment made by Vandieken et al. (2006) and Nickel et al (2008), who suggested that more ice-free stations in the northern Barents Sea supported higher of sulfate reduction than the more permanently ice-covered stations reflecting lower carbon export production.

4.2. Marine versus terrestrial organic matter contribution

Terrestrial organic carbon sources to the Laptev and East Siberian shelf and slope are riverine discharge and coastal erosion of ice core complex (Stein and Macdonald, 2004; Vonk et al., 2012; Rachold et al., 2004; Fahl and Nöthig, 2007; Semiletov, 1999). Marine organic carbon is derived from open-water production during the ice-free months, export of ice algae, and new production in polynyas (Sakshaug et al., 2004; Nitishinsky et al. (2007). Generally, marine productivity in the Laptev Sea is low and controlled by the nutrient concentrations derived from Atlantic water, but spring outflow from the Lena River provides an additional temporary land-derived nutrient source (Pivovarov et al., 1999; Sakshaug et al., 2004; Nitishinsky et al., 2007; Bourgeois et al., 2017) during late spring ice melt (Raymond et al., 2007). Terrestrial-derived nutrients can also affect marine productivity either directly by new

production, or indirectly, due to plankton production from remineralized terrestrial DOC/POC (Alling et al., 2012). In the eastern East Siberian and Chukchi Sea, the inflow of nutrient-rich Pacific water supports higher marine primary productivity (e.g., Grebmeier et al., 2006). Ice-rafted transport and bottom boundary layer transport are the two most important modes of particle transport (Wegner et al., 2005; Bauch et al., 2009). Since all sediments sampled in this study were fine-grained siltey clays and clayey silts, coarse-grained woody, ice-rafted material played only a minor role for deposition of organic matter on the outer shelf and slope sediment. The transport direction of inner shelf sediments has been suggested to follow the predominant atmospheric regime, which is thought to be linked to the Arctic Oscillation (AO) (Dimitrenko et al., 2008; Guay et al., 2001; Weingartner et al., 1999). During positive AO southwesterly winds lead to generally eastward transport and repeated inshore transport in the BBL, whereas negative AO favors southerly winds and a predominantly northward transport (Guay et al., 2001; Dmitrenko et al., 2008). Offshore transport of dissolved and particulate organic matter from the Lean delta to the north can occur with the Transpolar Drift, but terrestrial organic material is also transported eastward and obliquely offshore with the Siberian coastal current receiving additional organic material from the Indigirka and Kolyma rivers (Guo et al., 2007; Dudarev et al., 2006). East of 140ºE, the influence of Pacific-derived nutrient-rich water supporting marine production is stronger the further east and offshore the sampling stations are located (Semiletov et al., 2005) (Fig. 1).

Carbon degradation rates in the sediment across the whole Siberian shelf and slope reflect this temporally and spatially diverse distribution of nutrient availability, ice cover, sediment deposition, and current flow regime (Rachold et al., 2004; Dudarev et al., 2006; Semiletov et al., 2005; Sakshaug et al., 2004; Dmitrenko et al., 2005). The proportion of degradable marine-derived organic material at the eastern Stations 50 to 63 on the East Siberian shelf is higher than at the western stations in the Laptev Sea, in line with higher nutrient availability due to the Pacific influence. Ice-free conditions and the opening of water due to northward migration of ice shortly before the sampling likely supported new algal primary production at the shelf stations closest to land leading to enhanced export and deposition on the seafloor. During the time of sampling, only Stations 6 to 27 were ice-free, while Stations 23 and 24 had the longest ice-free condition before sampling. By contrast, Stations 30 to 63 were still covered by ice during sampling. New export of reactive organic material explains why O_2 uptake rates were the highest at stations 23 and 24 along the shelf to slope transect from station 1 to station 24 (Boetius and Damm, 1998). The same pattern as for

473 the O_2 uptake rates is also observed for the sulfate reduction rates indicating that reactive
474 organic matter is also buried below the oxygen penetration depth and mixed layer into the
475 sulfate-reducing zone. This indicates that a greater portion of reactive organic material is
476 buried closer to the Lena delta.

477 Published organic carbon budgets for the Arctic shelves infer an average burial
478 efficiency of about 1% of exported marine OC (Stein and Macdonald, 2004), while terrestrial
479 organic carbon, only accounting for about 10% of the organic carbon delivered to the Arctic
480 Ocean bottom, has been suggested to be preserved with about 90% efficiency (Macdonald et
481 al., 2015). Recently, Semiletov et al. (2016) compiled a large dataset indicating substantial
482 aragonite undersaturation of Arctic shelf bottom waters from the Laptev, the East Siberian,
483 and the Russian part of the Chukchi Sea, which was interpreted due to the remineralization of
484 terrestrial organic matter. The observation of strongest aragonite undersaturation in the
485 bottom waters supports a sediment-derived CO_2 source or a stagnant bottom boundary layer
486 (Semiletov et al., 2013). It is therefore possible that oxic carbon mineralization in the topmost
487 mm of sediment is a major CO_2 source for the overlying water.

488 In order to determine the mineralized proportion of terrestrial and marine organic
489 matter in the sediment directly, we use the DIC concentration and the carbon isotope
490 composition of DIC as indicators of remineralized organic matter in the sediment. The
491 remineralized fraction (F) of $DIC_{total,\ depth\ x}$ at the different sediment depths (x) was defined as

492 $$F = (DIC_{total,\ depth\ x} - DIC_{bottom\ water\ overlying\ core})/DIC_{total,\ depth\ x} \quad (3)$$

493 and this fraction was plotted against the respective carbon isotope composition of $DIC_{total,\ depth\ x}$ (Fig. 6B). The y-intercept of the linear regression was constrained by the carbon isotope
495 composition of DIC in the bottom water for the respective station so that the slope of the
496 regression line was the only unknown in this analysis. The gradients for each station yield the
497 average stable carbon isotope composition of the remineralized organic matter in the sediment
498 assuming no or very minor isotope fractionation during the oxidation of organic matter. This
499 calculation assumes that porewater removal of DIC by diagenetic processes such as $CaCO_3$
500 precipitation was minor and time-invariant, which is supported by the observation that Ca^{2+}
501 and Mg^{2+} porewater concentrations at these shelf and slope stations did not change
502 significantly with depth (Sun and Brüchert, unpubl. data). Fig. 6 shows exemplary gradients
503 of the regression for the six stations presented before and Table 3 lists the derived carbon
504 isotope compositions of remineralized organic matter for all stations. The range of $\delta^{13}C$ of

Biogeosciences Discuss., doi:10.5194/bg-2017-119, 2017
Manuscript under review for journal Biogeosciences
Discussion started: 13 April 2017

remineralized DIC varied between -18.8 ‰ ± 1.1 ‰ (Station 53) and -35.8‰ ± 3.0 ‰ (Station 1). The strongly ^{13}C-depleted isotope composition of -35.8 ‰ for remineralized DIC at Station 1 suggests the mineralization of strongly ^{13}C-depleted organic matter and possibly a strong contribution of terrestrial organic matter to carbon mineralization far offshore, in line with the very high DIC/NH_4^+ ratio of the porewaters at the slope stations. The potential existence of degradable terrestrial organic matter in slope sediments of 3000 m water depth is intriguing, since it would imply downslope transport and degradation of terrestrial organic matter. Northward off-shelf transport of terrestrial organic matter with the Transpolar Drift is a viable transport mechanism. The contribution of degradable terrestrial organic matter to DIC in lower slope sediments is also supported by the observation of terrestrially derived biomarkers in porewater DOC of central Arctic Ocean sediment analyzed by FT-ICRMS (Rossel et al., 2016) and deep-water sediment trap data in the central Arctic Ocean (Fahl and Nöthig, 2007), but requires further investigation.

The isotope composition of the remineralized DIC therefore reflects mineralization of a mixture of organic molecules of different origins – interpreted here as a mixture of terrestrial and marine-derived organic matter. For the following discussion, given the uncertainty of the organic matter origin in slope sediment, we exclude data from the slope stations and restrict the discussion to the use of the following end member compositions for the shelf stations. For the Laptev Sea shelf, we account for the fact that a fraction of the DIC used for marine production is derived from remineralized terrestrial DOC and POC in shelf waters. Alling et al. (2012) report $\delta^{13}C_{DIC}$ values for offshore DIC samples below the halocline varying between -2 and -4 ‰. We therefore use an isotope endmember for marine organic matter of -24 ‰ and an isotope composition of -28 ‰ for the terrestrial organic carbon contribution (Alling et al., 2010; Vonk et al., 2012). For the East Siberian Sea East of 140°E, the heaviest calculated isotope composition of remineralized DIC was -19 ‰ and is used here as the marine endmember (Station 53). The same carbon isotope composition of -28 ‰ as for the Laptev Sea was used as the terrestrial end member. The heavier marine $\delta^{13}C$ value in the East Siberian Sea is supported by the slightly heavier $\delta^{13}C_{DIC}$ values reported for the offshore East Siberian Sea, which vary between 0 and -2 ‰ (Alling et al., 2012).

The relative contributions of the terrestrial and marine organic carbon were then calculated with a linear two-endmember isotope model:

$$\delta^{13}C_{DIC,\ remineralized} = f_{terr} * \delta^{13}C_{terr\ OC} + f_{mar} * \delta^{13}C_{marine\ OC} \quad (4)$$

Biogeosciences Discuss., doi:10.5194/bg-2017-119, 2017
Manuscript under review for journal Biogeosciences
Discussion started: 13 April 2017

where f_{terr} and f_{mar} are the respective mass fractions of terrestrial and marine-derived organic carbon and $\delta^{13}C_{terrestrial}$ and $\delta^{13}C_{marine}$ reflect the isotope composition of these endmembers. The calculated mass fractions of the two endmembers are listed in Table 3. Based on this analysis the porewaters on the Laptev Sea shelf contain a significant proportion of terrestrially derived organic matter, comprising on average 36 % of the remineralized DIC. This proportion decreases to average values of 32% in the East Siberian Sea, in line with a greater marine production in this area due to the inflow of Pacific water (Semiletov et al., 2005, Dudarev et al., 2006; Naidu et al., 2000).

In order to derive specific degradation rates of the marine and terrestrial carbon fractions, the endmember mixing-based assessment of the marine and terrestrial organic carbon contributions to DIC were combined with the ^{35}S-sulfate reduction rates. Since ^{35}S-sulfate reduction rates constrain most of the anaerobic carbon mineralization of sediment buried below the oxygen penetration depth, our assessment includes, in contrast to earlier studies, the mineralization rates of terrestrial organic matter beyond the short time period of oxygen exposure in the topmost mm of sediment. Using sedimentation rates of 0.8 mm y^{-1} for the outer Laptev Sea (Strobl et al., 1988) and 1.4 mm y^{-1} for the outer East Siberian Sea (Bröder et al., 2016b), the recovered sediments record a time interval of 250 to 700 years since burial. Using the mass fractions of terrestrial and marine-derived organic carbon listed in Table 3, respective mineralization rates of the terrestrial and marine carbon fractions were calculated from the product of the mass fractions and the depth-integrated ^{35}S-sulfate reduction rates (Table 3). This approach is only applicable in combination with depth-integrated anaerobic carbon mineralization rates, but would be biased if used in combination with total oxygen uptake rates. The reason for this is that the depth of oxygen penetration varied only between a millimeter to little more than a centimeter on the shelf, whereas the corresponding DIC concentrations, even in the topmost centimeter of sediment, are affected by diffusive exchange along the 30 cm-long concentration profile smoothing out depth-dependent changes in the source signal of organic matter. It is therefore not possible to assess the relative fractions of terrestrial and marine organic matter mineralized for discrete depth intervals. Our combined radiotracer and DIC stable isotope approach suggests that both marine and terrestrial organic matter are degraded in the buried sediment and that both pools contribute to degradation products in anoxic buried sediment. This assessment is a significant modification to earlier studies by Boetius and Damm (1998) and Bourgeois et al. (2017), who

569 have described organic matter mineralization in Siberian Arctic sediments largely as a
570 function of oxygen uptake.

571 Carbon mineralization rates measured along the transect near 130ºE (Stations 1 through
572 24) reflect the influence of gradual offshore transport of terrestrial organic material (Bröder et
573 al., 2016a) (Fig. 7A, B). A comparison with the oxygen uptake rates reported by Boetius and
574 Damm (1998) indicates that all rates measured in 2014 were significantly higher than the rates
575 measured in 1993 by Boetius and Damm (1998). Although the different rates may reflect a
576 seasonal effect since Boetius and Damm's data were acquired later in the year than our data,
577 the increase may also point to higher organic carbon mass accumulation rates compared to 20
578 years ago, consistent with a decrease in the annual ice cover over the past 20 years in the
579 Arctic (Arrigo and van Dijken, 2011; Stroeve et al., 2012; Walsh et al., 2017). Whether these
580 rates reflect higher marine and/or terrestrial accumulation cannot be answered satisfyingly
581 with this data set.

582 Fig. 8A compares the oxygen uptake rate of the stations of this study with averaged
583 oxygen uptake rates from the literature for different shelf, slope, and abyssal plain
584 environments worldwide (Canfield et al., 2005). The data suggest that there is no significant
585 difference in the oxygen consumption rates between the Siberian shelf and slope and other
586 continental margin environments. ^{35}S-sulfate reduction rates in Sea Siberian slope sediment
587 are also comparable rates to those in other slope environments (Fig.7B and 8B), but the
588 sulfate reduction on the shelf are significantly lower, by a factor up to 15. Another difference
589 apparent from this comparison is the small range in sulfate reduction rates for the outer shelf
590 and continental slope sediments of the Siberian Arctic (Fig. 8B). This similarity is noteworthy
591 for several reasons: 1) it suggests that the kinetics of anaerobic carbon degradation in the shelf
592 and slope sediments reflect similar reactivity of the organic matter. This is surprising since
593 accumulation rates on the continental slope are significantly slower than on the outer shelf. 2)
594 The absolute magnitude of the sulfate reduction rates in shelf and slope sediment indicate
595 significant rates of organic matter mineralization long after burial consistent with the
596 substantial DIC flux and the strongly ^{13}C-depleted DIC carbon isotope composition. Overall,
597 the data that organic matter reactivity substantially changes during burial in shelf sediment,
598 but that the reactivity of transported organic matter that is exported to deep water across the
599 shelf does not decrease significantly supporting long-term slow mineralization rates in the
600 slope environment. Accumulation of the organic material on the slope may therefore be
601 related to rapid downslope transport of organic material or a rapid offshore transport, e.g., due

Biogeosciences Discuss., doi:10.5194/bg-2017-119, 2017
Manuscript under review for journal Biogeosciences
Discussion started: 13 April 2017

to transport with ice or as bottom nepheloid layers cascading from the shelf edge (Ivanov and Golovin, 2007).

4.3. Assessment of carbon burial efficiency

Reported ^{210}Pb-based sediment accumulation rates in outer shelf Siberian shelf sediment range between 0.05±0.02 g cm^{-2} y^{-1} in the Laptev Sea (Strobl et al., 1988) and 0.24±0.04 g cm^{-2} y^{-1} in the East Siberian Sea (Bröder et al., 2016b). Given surface sediment organic carbon concentration for this area between 1% and 1.5%, the resulting organic carbon mass accumulation rates vary between 1.1 mmol m^{-2} d^{-1} and 1.7 mmol m^{-2} d^{-1} for the Laptev Sea (area near Station 23) and 5.5 and 8.2 mmol m^{-2} d^{-1} in the East Siberian Sea (data for Station 63). We estimated the burial efficiency of terrestrial organic carbon from the ratio of the depth-integrated sulfate reduction rates relative to the ^{210}Pb mass accumulation rate of organic carbon. This treatment assumes that the reported organic carbon mass accumulation rates largely reflect the refractory component of organic matter. While it is possible that a fraction of terrestrial and marine organic matter is degraded on shorter time scales than captured by the ^{210}Pb method, we assume that the fraction of highly reactive terrestrial organic matter missed in this treatment is small. The resulting burial efficiency of the terrestrial carbon fraction is on average 69 ± 28 % in the Laptev Sea and 79 ± 6 % for the East Siberian Sea. We also calculated apparent degradation rate constants of organic matter assuming first order degradation kinetics for the time duration of sediment burial recorded in the sediment cores. For this assessment, we used the total depth-integrated anaerobic carbon mineralization determined from the combined manganese, iron, and sulfate reduction rates for the recovered sediment. The apparent annual degradation rate constant (k) was then calculated from

$$k_{terrestrial} = \frac{\left(-ln\frac{\int_0^{30} OC_{accumulation} - \int_0^{30} OC_{total\ mineralization}}{\int_0^{30} OC_{accumulation}}\right)}{t_{burial}} \quad (5)$$

where the integrals of $OC_{accumulation}$ and $OC_{mineralization}$ cover a period of 250 years to 700 years based on the ^{210}Pb mass accumulation rates. The resulting annual degradation rate constant ($k_{terrestrial}$) ranges between 1 x 10^{-4} y^{-1} and 5 x 10^{-4} y^{-1} averaging 1.5 x 10^{-4} y^{-1} in the Laptev Sea and between 8 x 10^{-5} and 3 x 10^{-4} y^{-1} averaging 1.2 x 10^{-4} y^{-1} in the East Siberian Sea.

A comparison of the total oxygen uptake with the C_{org} mass accumulation rates indicates that the ^{210}Pb-based C_{org} mass accumulation rates on the shelf are equal or

significantly lower than the oxygen uptake rates, with a discrepancy of up to a factor 10. Since the derivation of the ^{210}Pb-based C_{org} mass accumulation rates is based on the same depth range as our direct ^{35}S-based degradation rate measurements (30 cm of sediment, Vonk et al., 2012), C_{org} mass accumulation rates and degradation rate measurements cover the same time window of sediment burial. Temporal variation in sediment accumulation therefore cannot explain the discrepancy. In addition, methane seep sediments where upward transport of methane from deeper sediment layers contributed to oxygen uptake were excluded from this data set. The best explanation for the discrepancy is therefore that the ^{210}Pb-mass accumulation rates underestimate the true mass accumulation rate of highly reactive organic material and that this material is oxidized at the sediment surface. Based on the measured oxygen uptake rates this freshly deposited organic material has substantially higher degradation rates within the top mm of sediment as reflected by the steep O_2 gradients. ^{210}Pb-based organic carbon accumulation therefore reflects the long-term burial of less reactive organic material in the top 30 cm of sediment. Since anaerobic degradation processes prevail below the O_2 penetration depth, the measured burial efficiency of the accumulating organic material is therefore a function of the anaerobic bacterial degradation rather than the aerobic degradation efficiency. This conclusion has implications regarding the assessment of potential aerobic degradation of reactive terrestrial organic matter, since degradation of such material would have gone undetected with ^{210}Pb-based accumulation rate measurements.

4.4. The relative importance of iron, manganese and sulfate reduction for carbon degradation

There was a statistically significant positive correlation between the dissolved oxygen uptake and anaerobic carbon degradation rates by sulfate reduction with an r^2 of 0.72 ($P < 0.05$). This reflects the coupling of oxygen uptake to the oxidation of reduced inorganic metabolites (FeS and H_2S) produced during the anaerobic metabolism by sulfate reduction (e.g., Glud, 2008; Jørgensen and Kasten, 2006; Thamdrup, 2000; Berg et al., 2003) (Fig. 9). The slope of the regression line for the data set is 5.6±1.2 indicating that about 18% of the oxygen uptake is used for the oxidation of reduced manganese, ammonium, dissolved iron, and iron sulfides and elemental sulfur. This amount is close to and only slightly lower than the average 23% estimated for oxygenated coastal and continental shelf sediment (Canfield et al., 2005), and indicates that a substantial amount of the buried organic matter in Siberian shelf

664 sediment is oxidized anaerobically. The lower proportion of anaerobic respiration to aerobic
665 respiration compared to other shelf environments likely reflects the greater proportion of
666 highly reactive marine-derived organic material in the topmost millimeters of sediment.

667 Iron hydroxide surfaces have been inferred as important mineral surfaces for the
668 preservation of organic matter (Lalonde et al., 2012; Salvado et al., 2016). In all cases studied
669 here, the integrated net DIC production based on the porewater gradient of DIC, and the depth
670 profiles of iron reduction indicate co-existing heterotrophic and chemical iron reduction and
671 bacterial sulfate reduction. In addition, the porewater modelling results suggest that
672 bioturbation is an important sediment mixing process for some shelf stations. Organic matter
673 sorbed to mineral surfaces with deposition would thus have been subject to repeated
674 desorption as iron oxyhydroxides were reduced. While this observation does not contradict
675 the observation that some organic material is buried in association with iron oxyhydroxides,
676 the repeated cycling of the repeated redox cycling of the oxyhydroxides would prevent the
677 sorptive preservation of organic compounds.

678

679 **4.5. Regional estimates**

680 We present areal estimates of sediment carbon mineralization by extrapolating the
681 measured carbon mineralization rates over the outer Laptev Sea and East Siberian Sea shelf.
682 Such extrapolations of benthic carbon mineralization rates are notoriously difficult given
683 sediment heterogeneity and insufficient temporal data coverage of benthic carbon
684 mineralization rates. For this investigation, no near-shore or slope stations were included in
685 the assessment. The near-shore Siberian shelf environments are under much stronger
686 influence by coastal erosion and riverine discharge than the outer shelf stations and have
687 considerable longer open-water conditions than the outer shelf stations investigated here. In
688 addition, the sedimentation pattern in the near-shore environments is significantly more
689 diverse, which will affect sedimentation rates, grain size distribution, and carbon contents. For
690 this reason, we did not extend our extrapolations to the inner shelf environments. Some of
691 these inner shelf settings likely have much higher benthic carbon mineralization rates and
692 additional studies are required to constrain these better. Our coverage of the slope stations is
693 insufficient for meaningful spatial extrapolations. A large data set for this region has been
694 analyzed by Miller et al. (2016) and the reader is referred to this work.

We estimate the extent of the outer shelf area with depositional conditions comparable to those investigated here to cover approximately 280,000 km^2 of the Laptev Sea. For the East Siberian Sea, we estimate the respective area of the outer shelf to be 340,000 km^2. Due to the stronger terrestrial influence in the Laptev Sea, we calculated rates separately for the two shelf seas. The areal coverage with sediment stations was too sparse for statistically significant interpolations between stations that would give reliable spatial accounts of the gradients in rates between the stations. Instead, arithmetic averages of sediment mineralization rates and fluxes were calculated for these regions. Accepting the uncertainties in our assessment and data density, we estimate that the calculated areal rates could deviate by up to 50%. Table 5 lists the calculated rates based on the average flux calculated per square meter per day for oxygen uptake, DIC flux, bacterial sulfate, and total anaerobic carbon mineralization. For the latter three methods, the total flux was calculated for the marine and terrestrial component, respectively. The same analysis cannot be performed for the oxygen uptake for the reasons discussed in section 4.1. Since the major part of the oxygen uptake is likely associated with degradation of a highly reactive marine organic carbon component, the proportions calculated based on the $\delta^{13}C$ composition of DIC would not necessarily apply to the topmost mm of sediment. It is noteworthy to say that the rates calculated with our data set agree well with the O_2 uptake rates recently published by Bourgeois et al. (2017) for the Laptev Sea. Our calculations suggest that 5.2 and 10.4 Tg O_2 y^{-1}, respectively are taken up by the outer shelf sediment in the Laptev and East Siberian Sea, respectively, totaling 15.9 Tg y^{-1} for the whole investigated area. Anaerobic carbon mineralization based on DIC, ^{35}S-SRR and combined manganese, iron, and sulfate reduction range between 0.62 and 1.28 Tg y^{-1}. Of the total anaerobic carbon mineralization, between 0.25 and 0.48 Tg y^{-1} can be attributed to the oxidation of terrestrially derived organic material. This rate is five to ten times lower than the estimated annual water column degradation of particulate terrestrial organic matter in the Eastern Siberian Arctic shelf system of 2.5±1.6 Tg y^{-1} (Sanchez et al. 2011), and only between 0.5% and 2% of the annual organic carbon export from land (Stein and Macdonald, 2004; Vonk et al., 2012).

5. Conclusions

Directly measured carbon mineralization rates together with stable isotope and concentration data of East Siberian Arctic shelf and slope porewaters indicate that about one

third of the remineralized organic carbon in porewater DIC is derived from terrestrial organic matter. This conclusion confirms and extends previous observations that terrestrial organic carbon buried in Siberian shelf and slope sediment is not conservative (Semiletov et al., 2013; Karlsson et al., 2015; Bröder et al., 2016b). While mineralization of terrestrial organic material has been described for the water column and resuspended surface sediment, our data indicate that mineralization also proceeds long after burial in sediment. The estimated apparent carbon degradation rate constants of transformed terrestrial organic matter on the outer shelf are slow ($< 3 \times 10^{-4}$ y^{-1}) and the overall terrestrial carbon burial efficiency is relatively high (> 69 %), but lower than previously reported based on millennial-scale carbon burial rates (90 %, Stein and Macdonald, 2004). The low degradation rates are most apparent in the low bacterial sulfate reduction rates, which is the major anaerobic electron acceptor in these sediments. High porewater concentrations of dissolved iron and manganese testify to significant iron and manganese reduction that contributed up to 23.7% to the anaerobic carbon mineralization in these sediments, but only 2.3% to the total carbon mineralization. The pervasive presence of dissolved iron at all but one of the sediment stations in the eastern East Siberian Sea indicates the presence of abundant iron oxyhydroxides, which possibly play a role in the preservation of organic matter (Salvado et al., 2016; Lalonde et al., 2012).

The regional differences in the isotope composition of remineralized DIC and DIC/NH_4^+ ratios are in accordance with a greater proportion of terrestrially-derived organic matter in the Laptev Sea, but the absolute mineralization rates of the terrestrially derived organic matter were similar in both regions. This observation is important in light of a potential priming effect by marine-derived organic matter (Bianchi, 2011). Our data do not indicate that the larger marine fraction in the outer East Siberian Sea had a greater priming effect on terrestrial carbon than in the outer Laptev Sea, but an overall priming effect may deduced from the dual contribution of terrestrial and marine-derived organic matter to DIC. Area-integrated rates of carbon mineralization in the outer shelf sediments (0.29 to 0.48 Tg y^{-1}) represent about 0.5 % to 8 % of the annual terrestrial organic matter load to the Laptev and East Siberian Sea ranging from 6 Tg y^{-1} (Stein and Macdonald, 2004) to 22±8 to 44 Tg y^{-1} (Vonk et al., 2012). There are large uncertainties associated with these estimates, given that our calculations do not account for carbon mineralization of resuspended terrestrial organic material and likely higher rates of mineralization in the inner shelf sediments. Nevertheless, these data indicate that the contribution of the benthic DIC flux to the total CO_2 production in the outer Eastern Siberian Sea and Laptev Sea is small. This conclusion, however, does not

necessarily extend to the inner parts of the Laptev Sea and the western parts of the East Siberian Sea, where CO_2 supersaturation has been reported by Semiletov et al. (2012) and Pipko et al. (2011). Anderson et al (2009) estimated a DIC excess of 10 Tg C by evaluating data from the Laptev and East Siberian Seas collected in the summer of 2008 and suggested that this excess was caused mainly by terrestrial organic matter decomposition. Their estimate can be compared to our sediment oxygen uptake for the outer Laptev and East Siberian Sea shelf of almost 16 Tg y^{-1}, which would demand that 62.5 % of the oxygen uptake was due to terrestrial organic matter mineralization. However, the reported annual production of marine organic matter for the total Laptev and East Siberian Sea is about 46 Tg y^{-1} (Stein and Macdonald, 2004). Even if only half of this amount is produced in the outer shelf region and only another half of that amount was deposited, there would still be more than 10 Tg y^{-1} of reactive marine organic matter at the sediment surface. Our data would therefore suggest that at least in the more productive East Siberian Sea the pronounced aragonite undersaturation reported for bottom waters in the East Siberian Sea is due to aerobic mineralization of a significant amount of marine organic matter, which extends the assessment for the western Chukchi Sea and the central Arctic Ocean by Qi et al. (2017). It is apparent that these sediments play a major role in the recycling of marine organic carbon on the Arctic shelf. Future changes in marine production on the Siberian shelf under longer ice-free conditions (Arrigo and van Dijken, 2011) will likely change the relative proportions of degrading marine and terrestrial organic matter further so that this particular shelf system may in the future more strongly resemble that of other ice-free shelf-slope environments.

6. Acknowledgements

Funding for this investigation came from the K&A Wallenberg foundation, the Swedish Polarsekretariat, and the Bolin Centre for Climate Research at Stockholm University. Igor Semiletov acknowledge support from the Russian Government (No. 14.Z50.31.0012/03.19.2014). We would like to thank the members of the SWERUS-C3 consortium, the shipcrew on icebreaker Oden, and Heike Siegmund, Lina Hansson, Barkas Charalampos, and Dimitra Panagiotopoulou for help with the laboratory work. We dedicate this publication to our friend and colleague Vladimir Samarkin, who unfortunately passed away before publication of this work. This manuscript benefitted from discussions with

Patrick Crill, Örjan Gustafsson, Christoph Humborg, Julia Steinbach, Clint Miller, Marc Geibel, Emma Karlsson, Brett Thornton, Jorien Vonk, Leif Anderson, and Magnus Mörth.

List of Tables

List of figures

836 mixing model versus $\delta^{13}C_{DIC}$. The slope and y-intercept of the regression for each station are
837 shown in Table 3.

838

839 Fig. 7 A, B. Map of field area and sampling stations showing oxygen uptake rates in panel A
840 and depth-integrated sulfate reduction rates in panel B.

841

842 Fig. 8A. Water depth variation of sediment oxygen uptake. 8B: Water depth variation of
843 integrated ^{35}S-sulfate reduction rates (0-30 cm sediment depth). For reference average rates of
844 abyssal plain, continental rise, slope, and shelf sediments, deposition and non-depositional,
845 are shown for reference.

846

847 Fig. 9. Crossplot of diffusive oxygen uptake and integrated sulfate reduction rates. The black
848 line is the linear regression and yielded a y-intercept of 2.1 mmol m^{-2} d^{-1} and a slope of 5.55.
849 Blue and red lines show the 95% and 99% confidence interval.

850

851

Biogeosciences Discuss., doi:10.5194/bg-2017-119, 2017
Manuscript under review for journal Biogeosciences
Discussion started: 13 April 2017

852 **7. References**

853

854 Alling, V., Sanchez-Garcia, L., Porcelli, D., Pugach, S., Vonk, J. E., van Dongen, B., Mörth,
855 C.-M., Anderson, L. G., Sokolov, A., Andersson, P., Humborg, C., Semiletov, I., and
856 Gustafsson, Ö.: Non-conservative behavior of dissolved organic carbon across the Laptev and
857 East Siberian seas, Global Biogeochemical Cycles, 24, 10.1029/2010gb003834, 2010.

858 Alling, V., Porcelli, D., Mörth, C. M., Anderson, L. G., Sanchez-Garcia, L., Gustafsson, Ö.,
859 Andersson, P. S., and Humborg, C.: Degradation of terrestrial organic carbon, primary
860 production and out-gassing of CO_2 in the Laptev and East Siberian Seas as inferred from $\delta^{13}C$
861 values of DIC, Geochimica et Cosmochimica Acta, 95, 143-159, 2012.

862 Anderson LG, Jutterström S, Hjalmarsson S, Wahlstrom I, Semiletov IP. Out-gassing of CO_2
863 from Siberian Shelf seas by terrestrial organic matter decomposition. Geophysical Research
864 Letters, **36**, L20601, 2009.

865 Arrigo, K. R., and van Dijken, G. L.: Secular trends in Arctic Ocean net primary production,
866 Journal of Geophysical Research: Oceans, 116, 10.1029/2011JC007151, 2011.

867 Bauch, D., Dmitrenko, I., Kirillov, S., Wegner, C., Hölemann, J., Pivovarov, S., Timokhov,
868 L., and Kassens, H.: Eurasian Arctic shelf hydrography: Exchange and residence time of
869 southern Laptev Sea waters, Continental Shelf Research, 29, 1815-1820, 2009.

870 Berg, P., Petersen-Risgaard, N., and Rysgaard, S.: Interpretation and measured concentration
871 profiles in sediment pore water, Limnology and Oceanography, 43, 1500-1510, 1998.

872 Berg, P., Rysgaard, S., and Thamdrup, B.: Dynamic modeling of early diagenesis and nutrient
873 cycling. A case study in an Arctic marine sediment, Amer. J. Sci, 303, 906-955, 2003.

874 Boetius, A., and Damm, E.: Benthic oxygen uptake, hydrolytic potentials and microbial
875 biomass at the Arctic continental slope, Deep Sea Research Part I: Oceanographic Research
876 Papers, 45, 239-275, 1998.

877 Boudreau, B. P.: Diagenetic models and their implementation, Springer Verlag, 414 pp.,
878 1996.

879 Bourgeois, S., Archambault, P., and Witte, U.: Organic matter remineralization in marine
880 sediments: A Pan-Arctic synthesis, Global Biogeochemical Cycles, 31, 190-213, 2017.

881 Bröder, L.-M., Tesi, T., Salvado, J. A., Semiletov, I., Dudarev, O. V., and Gustafsson, Ö.:
882 Fate of terrigeneous organic matter across the Laptev Sea from the mouth of the Lena River to
883 the deep sea of the Arctic interior, Biogeosciences, 13, 5003-5019, 2016a.

884 Bröder, L., Tesi, T., Andersson, A., Eglinton, T. I., Semiletov, I. P., Dudarev, O. V., Roos, P.,
885 and Gustafsson, Ö.: Historical records of organic matter supply and degradation status in the
886 East Siberian Sea, Organic Geochemistry, 91, 16-30, 2016b.

887 Canfield, D. E., Kristensen, E., and Thamdrup, B.: Aquatic geomicrobiology, Advances in
888 marine biology, 48, 2005.

889 Dmitrenko, I. A., Tyshko, K. N., Kirillov, S. A., Eicken, H., Hölemann, J. A., and Kassens,
890 H.: Impact of flaw polynyas on the hydrography of the Laptev Sea, Global and Planetary
891 Change, 48, 9-27, 2005.

892 Dmitrenko, I. A., Kirillov, S. A., and Tremblay, L. B.: The long -term and interannual
893 variability of summer fresh water storage over the eastern Siberian shelf: Implication for
894 climatic change, Journal of Geophysical Research: Oceans, 113, doi: 10.1029/2007JC004304,
895 2008.

896 Dudarev, O. V., Semiletov, I. P., and Charkin, A. N.: Particulate material composition in the
897 Lena River-Laptev Sea system: Scales of heterogeneities. In: Doklady Earth Sciences, 6,
898 1000-1005, 2006.

899 Fahl, K., and Nöthig, E.-M.: Lithogenic and biogenic particle fluxes on the Lomonosov Ridge
900 (central Arctic Ocean) and their relevance for sediment accumulation: Vertical vs. lateral
901 transport, Deep Sea Research Part I: Oceanographic Research Papers, 54, 1256-1272, 2007.

902 Glud, R. N.: Oxygen dynamics of marine sediments, Mar. Biol. Res., 4, 243-289, 2008.

903 Grebmeier, J. M., Cooper, L. W., Feder, H. M., and Sirenko, B. I.: Ecosystem dynamics of the
904 Pacific-influenced Northern Bering and Chukchi Seas in the Amerasian Arctic, Progress in
905 Oceanography, 71, 331-361, 2006.

906 Guay, C. K., Falkner, K. K., Muench, R. D., Mensch, M., Frank, M., and Bayer, R.: Wind -
907 driven transport pathways for Eurasian Arctic river discharge, Journal of Geophysical
908 Research: Oceans, 106, 11469-11480, 2001.

909 Guo, L., Ping, C. L., and Macdonald, R. W.: Mobilization pathways of organic carbon from
910 permafrost to arctic rivers in a changing climate, Geophysical Research Letters, 34, 2007.

911 Hall, P. O. J., and Aller, R. C.: Rapid, small-volume flow injection analysis for ΣCO_2 and
912 NH_4^+ in marine and freshwaters, Limnology and Oceanography, 37, 1113-1119, 1992.

913 Hugelius, G., Strauss, J., Zubrzycki, S., Harden, J. W., Schuur, E. A. G., Ping, C. L.,
914 Schirrmeister, L., Grosse, G., Michaelson, G. J., Koven, C. D., O'Donnell, J. A., Elberling, B.,
915 Mishra, U., Camill, P., Yu, Z., Palmtag, J., and Kuhry, P.: Estimated stocks of circumpolar
916 permafrost carbon with quantified uncertainty ranges and identified data gaps,
917 Biogeosciences, 11, 6573-6593, 2014.

918 Ivanov, V. V. and Golovin, P. N.: Observations and modeling of dense water cascading from
919 the northwestern Laptev Sea shelf, Journal of Geophysical Research: Oceans, 112, 2007.

920 Jørgensen, B. B.: A comparison of methods for the quantification of bacterial sulfate
921 reduction in coastal marine sediments: I. Measurement with radiotracer techniques,
922 Geomicrobiology Journal, 1, 11-27, 1978.

923 Jørgensen, B. B., and Kasten, S.: Sulfur and methane oxidation, in: Marine Geochemistry,
924 Second Edition ed., edited by: Schulz, H. D., and Zabel, M., Springer Verlag, Berlin
925 Heidelberg, 271-309, 2006.

926 Kallmeyer, J., Ferdelman, T. G., Weber, A., Fossing, H., and Jørgensen, B. B.: Evaluation of
927 a cold chromium distillation procedure for recovering very small amounts of radiolabeled
928 sulfide related to sulfate reduction measurements., Limnol. Oceanog. Methods, 2, 171-180,
929 2004.

930 Karlsson, E. S., Brüchert, V., Tesi, T., Charkin, A., Dudarev, O., Semiletov, I., and
931 Gustafsson, Ö.: Contrasting regimes for organic matter degradation in the East Siberian Sea
932 and the Laptev Sea assessed through microbial incubations and molecular markers, Marine
933 Chemistry, 170, 11-22, 2015.

Koven, C. D., Lawrence, D. M., and Riley, W. J.: Permafrost carbon-climate feedback is sensitive to deep soil carbon decomposability but not deep soil nitrogen dynamics, Proceedings of the National Academies of Science, 112, 3752-3757, 2015.

Lalonde, K., Mucci, A., Ouellet, A., and Gelinas, Y.: Preservation of organic matter in sediments promoted by iron, Nature, 483, 198-200, 2012.

Macdonald, R. W., and Gobeil, C.: Manganese Sources and Sinks in the Arctic Ocean with Reference to Periodic Enrichments in Basin Sediments, Aquatic Geochemistry, 18, 565-591, 2012.

Macdonald, R. W., Kuzyk, Z. Z. A., and Johannessen, S. C.: The vulnerability of Arctic shelf sediments to climate change, Environmental Reviews, 1-19, 2015.

McGuire, A. D., Anderson, L. G., Christensen, T. R., Dallimore, S., Guo, L., Hayes, D. J., Heimann, M., Lorenson, T. D., Macdonald, R. W., and Roulet, N.: Sensitivity of the carbon cycle in the Arctic to climate change, Ecological Monographs, 79, 523-555, 2009.

McTigue, N., Gardner, W., Dunton, K., and Hardison, A.: Biotic and abiotic controls on co-occurring nitrogen cycling processes in shallow Arctic shelf sediments, Nature Communications, 7, 2016.

Miller, C. M., Dickens, G. R., Jakobsson, M., Johansson, C., Koshurnikov, A., O'Regan, M., Muschitiello, F., Stranne, C., and Mörth, C.-M.: Low methane concentrations in sediment along the continental slope north of Siberia: Inference from pore water geochemistry, Biogeosciences Discussions, doi:10.5194/bg-2016-308, 2016.

Naidu, A. S., Cooper, L. W., Finney, B. P., Macdonald, R. W., Alexander, C., and Semiletov, I. P.: Organic carbon isotope ratios ($\delta^{13}C$) of Arctic Amerasian Continental shelf sediments. International Journal of Earth Sciences, 89, 522-532, 2000.

Nickel, M., Vandieken, V., Brüchert, V., and Jørgensen, B. B.: Microbial Mn(IV) and Fe(III) reduction in northern Barents Sea sediments under different conditions of ice cover and organic carbon deposition, Deep Sea Research Part II: Topical Studies in Oceanography, 55, 2390-2398, 2008.

Nitishinsky, M., Anderson, L. G., and Hölemann, J. A.: Inorganic carbon and nutrient fluxes on the Arctic Shelf, Continental Shelf Research, 27, 1584-1599, 2007.

963 Pipko, I., Semiletov I.P., Pugach S.P., Wahlstrom I., Anderson L.G. Interannual variability of
964 air-sea CO_2 fluxes and carbon system in the East Siberian Sea. Biogeosciences, **8**, 1987-2007,
965 2011.

966 Pivovarov, S., Hölemann, J., Kassens, H., Antonow, M., and Dmitrenko, I.: Dissolved
967 oxygen,silicon,phosphorous and suspended matter concentrations during the spring breakup
968 of the Lena River, in: Land–Ocean Systems in the Siberian Arctic:Dynamics and History,
969 edited by: Kassens, H., Bauch, H. A., Dmitrenko, I., Eicken, H., Hubberten, H.-W., Melles,
970 M., Thiede, J., and Timokhov, L., Springer, Berlin, 251-264, 1999.

971 Qi, D., Chen, L., Chen, B., Gao, Z., Zhong, W., Feely, R. A., Anderson, L. G., Sun, H., Chen,
972 J., Chen, M., Zhan, L., Zhang, Y., and Cai, W.-J.: Increase in acidifying water in the western
973 Arctic Ocean, Nature Clim. Change, 7, 195-199, 2017.

974 Rachold, V., Eicken, H., Gordeev, V., Grigoriev, M. N., Hubberten, H.-W., Lisitzin, A. P.,
975 Shevchenko, V., and Schirrmeister, L.: Modern terrigenous organic carbon input to the Arctic
976 Ocean, in: The organic carbon cycle in the Arctic Ocean, Springer, 33-55, 2004.

977 Rasmussen, H., and Jørgensen, B. B.: Microelectrode studies of seasonal oxygen uptake in a
978 coastal sediment: Role of molecular diffusion, Marine ecology progress series. Oldendorf, 81,
979 289-303, 1992.

980 Raymond, P. A., McClelland, J., Holmes, R., Zhulidov, A., Mull, K., Peterson, B., Striegl, R.,
981 Aiken, G., and Gurtovaya, T.: Flux and age of dissolved organic carbon exported to the Arctic
982 Ocean: A carbon isotopic study of the five largest arctic rivers, Global Biogeochemical
983 Cycles, 21, 10.1029/2007GB002983, 2007.

984 Rekant, P., Bauch, H. A., Schwenk, T., Portnov, A., Gusev, E., Spiess, V., Cherkashov, G.,
985 and Kassens, H.: Evolution of subsea permafrost landscapes in Arctic Siberia since the Late
986 Pleistocene: a synoptic insight from acoustic data of the Laptev Sea, Arktos, 1,
987 10.1007/s41063-015-0011-y, 2015.

988 Rossel, P. E., Bienhold, C., Boetius, A., and Dittmar, T.: Dissolved organic matter in pore
989 water of Arctic Ocean sediments: Environmental influence on molecular composition,
990 Organic Geochemistry, 97, 41-52, 2016.

991 Sakshaug, E.: Primary and secondary production in the Arctic Seas, in: The organic carbon
992 cycle in the Arctic Ocean, Springer, 57-81, 2004.

993 Salvadó, J. A., Tesi, T., Andersson, A., Ingri, J., Dudarev, O. V., Semiletov, I. P., and
994 Gustafsson, Ö.: Organic carbon remobilized from thawing permafrost is resequestered by
995 reactive iron on the Eurasian Arctic Shelf, Geophysical Research Letters, 42, 8122-8130,
996 2015.

997 Sánchez-García, L., Alling, V., Pugach, S., Vonk, J., van Dongen, B., Humborg, C., Dudarev,
998 O., Semiletov, I., and Gustafsson, Ö.: Inventories and behavior of particulate organic carbon
999 in the Laptev and East Siberian seas, Global Biogeochemical Cycles, 25,
1000 10.1029/2010gb003862, 2011.

1001 Savvichev, A., Rusanov, I., Pimenov, N., Zakharova, E., Veslopolova, E., Lein, A. Y., Crane,
1002 K., and Ivanov, M.: Microbial processes of the carbon and sulfur cycles in the Chukchi Sea,
1003 Microbiology, 76, 603-613, 2007.

1004 Schuur, E. A. G., McGuire, A. D., Schadel, C., Grosse, G., Harden, J. W., Hayes, D. J.,
1005 Hugelius, G., Koven, C. D., Kuhry, P., Lawrence, D. M., Natali, S. M., Olefeldt, D.,
1006 Romanovsky, V. E., Schaefer, K., Turetsky, M. R., Treat, C. C., and Vonk, J. E.: Climate
1007 change and the permafrost carbon feedback, Nature, 520, 171-179, 2015.

1008 Seeberg-Elverfeldt, J., Schlüter, M., Feseker, T., and Kölling, M.: Rhizon sampling of
1009 porewaters near the sediment-water interface of aquatic systems, Limnol. Oceanogr. Methods,
1010 3, 361-371, 2005.

1011 Semiletov, I., Dudarev, O., Luchin, V., Charkin, A., Shin, K.-H., and Tanaka, N.: The East
1012 Siberian Sea as a transition zone between Pacific-derived waters and Arctic shelf waters,
1013 Geophysical Research Letters, 10.1029/2005GL022490, 2005.

1014 Semiletov, I., Pipko, I., Gustafsson, Ö., Anderson, L. G., Sergienko, V., Pugach, S., Dudarev,
1015 O., Charkin, A., Gukov, A., Broder, L., Andersson, A., Spivak, E., and Shakhova, N.:
1016 Acidification of East Siberian Arctic Shelf waters through addition of freshwater and
1017 terrestrial carbon, Nature Geoscience, 9, 361-365, 2016.

1018 Semiletov I.P., Shakhova, N.E, Pipko, I.I.: Space-time dynamics of carbon and environmental
1019 parameters related to carbon dioxide emissions in the Buor-Khaya Bay and adjacent part of
1020 the Laptev Sea. Biogeosciences, **10**, 5977-5996, 2013.

1021 Semiletov I.P., Pipko I.I., Shakhova N.E., Dudarev O.V., Pugach S.P., Charkin A.N., McRoy

1022 C.P., Kosmach D., and Ö. Gustafsson.: Carbon transport by the Lena River from its
1023 headwaters to the Arctic Ocean, with emphasis on fluvial input of terrestrial particulate
1024 organic carbon vs. carbon transport by coastal erosion. Biogeosciences, **8**, 2407-2426, 2011.

1025 Semiletov, I.P., Destruction of the coastal permafrost ground as an important factor in
1026 biogeochemistry of the Arctic Shelf waters, Trans. (Doklady) Russian Acad. Sci., 368, 679-
1027 682, 1999 (translated into English).

1028 Stein, R., and Macdonald, R. W.: The Organic Carbon Cycle in the Arctic Ocean, Springer-
1029 Verlag, Berlin, 382 pp., 2004.

1030 Strobl, C., Schulz, V., Vogler, S., Baumann, S., Kassens, H., Kubik, P. W., Suter, M., and
1031 Mangini, A.: Determination of depositional beryllium-10 fluxes in the area of the Laptev Sea
1032 and beryllium-10 concentrations in water samples of high northern latitudes, in: Land-Ocean
1033 Systems in the Siberian Arctic: Dynamics and History, edited by: Kassens, H., Bauch, H. A.,
1034 Dmitrenko, I., Eicken, H., Hubberten, H.-W., Melles, M., Thiede, J., and Timokhov, L.,
1035 Springer, Berlin, 515-532, 1998.

1036 Tarnocai, C., Canadell, J. G., Schuur, E. A. G., Kuhry, P., Mazhitova, G., and Zimov, S.: Soil
1037 organic carbon pools in the northern circumpolar permafrost region, Global Biogeochemical
1038 Cycles, 23, 10.1029/2008gb003327, 2009.

1039 Tesi, T., Semiletov, I., Hugelius, G., Dudarev, O., Kuhry, P., and Gustafsson, Ö.:
1040 Composition and fate of terrigenous organic matter along the Arctic land–ocean continuum in
1041 East Siberia: Insights from biomarkers and carbon isotopes, Geochimica et Cosmochimica
1042 Acta, 133, 235-256, 2014.

1043 Tesi, T., Semiletov, I., Dudarev, O., Andersson, A., and Gustafsson, Ö.: Matrix association
1044 effects on hydrodynamic sorting and degradation of terrestrial organic matter during cross-
1045 shelf transport in the Laptev and East Siberian shelf seas, Journal of Geophysical Research:
1046 Biogeosciences, 121, 731-752, 2016.

1047 Thamdrup, B.: Bacterial manganese and iron reduction in aquatic sediments, Advances in
1048 Microbial Ecology, 16, 41-84, 2000.

1049 Arrigo, K. R., and van Dijken, G. L.: Secular trends in Arctic Ocean net primary production,
1050 Journal of Geophysical Research: Oceans, 116, 10.1029/2011JC007151, 2011.

1051 Hugelius, G., Strauss, J., Zubrzycki, S., Harden, J. W., Schuur, E. A. G., Ping, C. L.,
1052 Schirrmeister, L., Grosse, G., Michaelson, G. J., Koven, C. D., O'Donnell, J. A., Elberling, B.,
1053 Mishra, U., Camill, P., Yu, Z., Palmtag, J., and Kuhry, P.: Estimated stocks of circumpolar
1054 permafrost carbon with quantified uncertainty ranges and identified data gaps,
1055 Biogeosciences, 11, 6573-6593, 2014.

1056 Qi, D., Chen, L., Chen, B., Gao, Z., Zhong, W., Feely, R. A., Anderson, L. G., Sun, H., Chen,
1057 J., Chen, M., Zhan, L., Zhang, Y., and Cai, W.-J.: Increase in acidifying water in the western
1058 Arctic Ocean, Nature Clim. Change, 7, 195-199, 2017.

1059 Sánchez-García, L., Alling, V., Pugach, S., Vonk, J., van Dongen, B., Humborg, C., Dudarev,
1060 O., Semiletov, I., and Gustafsson, Ö.: Inventories and behavior of particulate organic carbon
1061 in the Laptev and East Siberian seas, Global Biogeochemical Cycles, 25,
1062 10.1029/2010gb003862, 2011.

1063 Vandieken, V., Nickel, M., and Jørgensen, B. B.: Carbon mineralization in Arctic sediments
1064 northeast of Svalbard: (Mn(IV) and Fe(III) reduction as principal anaerobic respiratory
1065 pathways, Marine Ecology Progress Series, 322, 15-27, 2006.

1066 Vonk, J. E., Sanchez-Garcia, L., van Dongen, B. E., Alling, V., Kosmach, D., Charkin, A.,
1067 Semiletov, I. P., Dudarev, O. V., Shakhova, N., Roos, P., Eglinton, T. I., Andersson, A., and
1068 Gustafsson, O.: Activation of old carbon by erosion of coastal and subsea permafrost in Arctic
1069 Siberia, Nature, 489, 137-140.

1070 Wegner, C., Hölemann, J. A., Dmitrenko, I., Kirillov, S., and Kassens, H.: Seasonal variations
1071 in Arctic sediment dynamics—evidence from 1-year records in the Laptev Sea (Siberian
1072 Arctic), Global and Planetary Change, 48, 126-140, 2005.

1073 Wegner, C., Bauch, D., Hölemann, J. A., Janout, M. A., Heim, B., Novikhin, A., Kassens, H.,
1074 and Timokhov, L.: Interannual variability of surface and bottom sediment transport on the
1075 Laptev Sea shelf during summer, Biogeosciences, 10, 1117-1129, 2013.

1076 Weingartner, T. J., Danielson, S., Sasaki, Y., Pavlov, V., and Kulakov, M.: The Siberian
1077 Coastal Current: A wind- and buoyancy-forced Arctic coastal current, Journal of Geophysical
1078 Research: Oceans, 104, 29697-29713, 1999.

1079

Biogeosciences Discuss., doi:10.5194/bg-2017-119, 2017
Manuscript under review for journal Biogeosciences
Discussion started: 13 April 2017

1080

1081

Biogeosciences Discuss., doi:10.5194/bg-2017-119, 2017
Manuscript under review for journal Biogeosciences
Discussion started: 13 April 2017

Biogeosciences
Discussions
Open Access
EGU

1082

Table 1. Physical and chemical bottom characteristics

Station	Latitude °N	Longitude °E	Date	Water depth	Ice cover	Bottom water salinity	Bottom water temperature	Bottom water O_2 concentration	Bottom water NH_4^+ concentration	Bottom water DIC above sediment	$\delta^{13}C$ DIC bottom water	Sediment description
			Month/Day/Year	m	%	‰	°C	µmol/L	µmol/L	µmol/L	‰ vs. VPDB	
1	78.942	125.243	7/15/2014	3146	50 - 75	34.9	-0.9	271.9	1.65	2151.5	-0.5	clay, chocolate brown
2	78.581	125.607	7/16/2014	2900	25 - 50	34.9	-0.9	275.0		n.a.	n.a.	clay, chocolate-brown
3	78.238	126.150	7/16/2014	2601	< 25	34.9	-0.9	280.0		n.a.	n.a.	clay, chocolate-brown
4	77.855	126.664	7/16/2014	2106	< 25	34.9	-0.8	289.4	1.81	2164.5	-1.6	clay, chocolate-brown
6	77.142	127.378	7/17/2014	89	0.0	34.6	-1.8	327.0	1.30	2213.0	-2.2	clay, top 3 cm brown, then gray, fauna on top of sediment
23	76.171	129.333	7/22/2014	56	0.0	34.2	-1.8	303.2	1.34	2246.3	-3.2	silty clay, top 4 cm brown, then gray, brittle stars
24	75.599	129.558	7/24/2014	46	0.0	34.0	-1.7	283.8	0.89	2244.1	-2.0	silty clay, top 4 cm brown, then gray
27	76.943	132.229	7/23/2014	44	0.0	34.2	-1.8	332.3	0.94	2595.0	-6.5	silty clay, top 2 cm brown, then gray, fluffy surface layer, brittle stars
30	78.181	138.354	7/24/2014	69	0.0	34.1	-1.6	334.8	0.79	2178.4	-3.7	silty clay, top 4 cm brown, then gray
31	79.396	135.497	7/25/2014	3056	0.0	34.9	-0.9	270.9	0.74	2161.7	n.a.	clay, chocolate brown
35	78.600	137.061	7/26/2014	541	0.0	34.9	0.4	288.1	0.43	2183.7	n.a.	clay top 15cm brown, fluffy, inhomogeneous, surface-dwelling fauna
37	78.521	137.170	7/26/2014	205	0.0	34.7	0.0	295.4	0.89	2171.1	n.a.	clay, top 5cm brown, then gray
40	77.670	144.668	7/27/2014	45	0.0	31.5	-1.3	190.3	0.53	2213.7	-1.6	silty clay, top 3cm brown, then gray, brittle stars
43	76.780	147.791	7/28/2014	42	25-50	30.1	-1.2	256.4	0.61	2086.7	n.a.	silty clay to clayey silt, top 2cm brown, then gray, some small durface-dwelling animals
45	76.416	148.115	7/29/2014	40	< 50	29.1	-1.3	319.9	0.57	2576.0	-2.1	silty clay to clayey silt, 2cm brown, then gray black, rather stiff
48	76.615	153.345	7/30/2014	49	> 75	30.6	-1.6	315.9	0.50	2075.1	-2.2	silty clay to clayey silt, top 3cm brown, then grayblack
50	75.764	158.529	8/1/2014	44	> 75	31.1	-1.4	311.0	0.51	2068.7	-2.1	silty clay to clayet silt, top 2cm brown, then grayblack
53	74.957	161.088	8/2/2014	47	> 75	31.0	-1.6	253.3	0.16	2086.1	-2.5	silty clay to clayey silt, top 3 cm brown, then 3 cm gray, then grayblack
58	74.440	166.050	8/4/2014	54	> 75	31.4	-1.7	254.3	0.65	2154.9	-1.5	silty clay to clayey silt, slightly resuspended, top 2 cm brown, then gray, soft
63	74.685	172.361	8/7/2014	67	> 75	32.4	-1.4	186.0	0.61	2240.8	-2.2	silty clay to clayey silt, top 1cm brown, then gray

Biogeosciences Discuss., doi:10.5194/bg-2017-119, 2017
Manuscript under review for journal Biogeosciences
Discussion started: 13 April 2017

Biogeosciences Discussions
Open Access
EGU

1083

Table 2. Summary of bottom water concentrations, carbon isotope composition of bottom water DIC and remineralized DIC, DIC/NH_4^+ ratios, O_2 uptake, and integrated ^{35}S-sulfate reduction rates

Station	Bottom water NH_4^+ above sediment	Bottom water DIC above sediment	δ^{13}C DIC bottom water	mean O_2 penetration depth	mean O depth	O_2 uptake (modelled)	^{35}S-SRR (0-30 cm) duplicates	DIC flux (modelled)	Average porewater DIC/NH_4^+
	µmol/L	µmol/L	‰ vs. VPDB	mm	µmol/L	mmol m^{-2} d^{-1}	mmol m^{-2} d^{-1}	mmol m^{-2} d^{-1}	
1	1.6	2151.5	-0.5	> 60	217	1.48 ± 0.08	0.05 / 0.21	-0.11	
2	n.a.	n.a.	n.a.	> 60	213	1.32 ± 0.05			
3	n.a.	n.a.	n.a.	> 60	194	0.81 ± 0.06			
4	1.8	2164.5	-1.6	> 60	89	1.32 ± 0.05	0.17 / 0.17	-0.15	
6	1.3	2213.0	-2.2	36	0	2.61 ± 0.01	0.03 / 0.05	-0.08	
23	1.3	2246.3	-3.2	13	0	10.00 ± 0.09	0.56	-0.12	13
24	0.9	2244.1	-2.0	10	0	7.95 ± 0.14		-0.22	10
27	0.9	2595.0	-6.5	16	0	3.75 ± 0.08	0.37 / 0.20	-0.27	12
30	0.8	2178.4	-3.7	16	0	2.61 ± 0.11	0.06 / 0.03	-0.12	15
31	0.7	2161.7	n.a.	> 60	194	1.78 ± 0.07			
35	0.4	2183.7	n.a.	> 60	30	2.43 ± 0.32			
37	0.9	2171.1	n.a.	44	0	2.51 ± 0.10			
Average Laptev Sea shelf						**4.20**	**0.19**	**0.16**	**12**
40	0.5	2213.7	-1.6	12	0	4.62 ± 0.08	0.33 / 0.24	-0.19	16
43	0.6	2086.7	n.a.	13	0	4.7 ± 0.10			
45	0.6	2576.0	-2.1	10	0	4.02 ± 0.10	0.23 / 0.19	-0.37	13
48	0.5	2075.1	-2.2	5	0	9.14 ± 0.22	0.68 / 0.53	-0.71	10
50	0.5	2068.7	-2.1	9	0	8.65 ± 0.43	1.32 / 1.40	-1.01	12
53	0.2	2086.1	-2.5	10	0	4.53 ± 0.08	0.10 / 0.17	-0.20	14
58	0.7	2154.9	-1.5	3	0	11.49 ± 0.52	1.01	-1.27	24
63	0.6	2240.8	-2.2	4	0	10.72 ± 0.15	1.41	-1.35	12
Average East Siberian Sea shelf								**0.73**	**14**

Biogeosciences Discuss., doi:10.5194/bg-2017-119, 2017
Manuscript under review for journal Biogeosciences
Discussion started: 13 April 2017

Biogeosciences Discussions Open Access EGU

1084

1085

Table 3. Calculated carbon isotope composition of reminaralized DIC and mass fractions of marine and terrestrial end member and corresponding terrestrial carbon degradation rates based on ^{35}S-SRR and DIC flux

Station	Average $\delta^{13}C_{DIC}$ remineralized	Marine end member	Terrestrial end member	^{35}S-SRR-based terrestrial degradation rate	DIC-based terrestrial degradation rate
	‰ vs. VPDB	Mass fraction		mmol m^{-2} d^{-1}	mmol m^{-2} d^{-1}
1	-32.5	0.0	1.0	0.13	0.11
4	-24.7	0.73	0.27	0.05	0.04
6	-25.1	0.65	0.35	0.01	0.03
23	-24.5	0.78	0.22	0.12	0.03
24	-24.7	0.73	0.27		0.06
27	-25.4	0.58	0.42	0.12	0.11
30	-28.5	0.00	1.00	0.05	0.13
Average Laptev Sea shelf	**-25.6**	**0.53**	**0.47**	**0.08**	**0.07**
40	-21.4	0.72	0.28	0.08	0.05
45	-22.2	0.63	0.37	0.08	0.14
48	-23.0	0.54	0.46	0.28	0.32
50	-24.0	0.43	0.57	0.77	0.57
53	-18.8	1.00	0.00	0.00	0.00
58	-22.6	0.59	0.41	0.42	0.53
63	-20.3	0.84	0.16	0.25	0.22
Average East Siberian Sea shelf	**-21.8**	**0.68**	**0.32**	**0.27**	**0.26**

Biogeosciences Discuss., doi:10.5194/bg-2017-119, 2017
Manuscript under review for journal Biogeosciences
Discussion started: 13 April 2017

Table 4 Anaerobic rates of carbon mineralization by manganese, iron, and sulfate reduction

	Net Fe^{2+} production	Net Mn^{2+} production	C-equivalent Fe + Mn reduction	^{35}S-Sulfate reduction	C-equivalents total anaerobic mineralization	Oxygen uptake	% Fe + Mn reduction of total anaerobic mineralization	Percentage anaerobic C mineralization of total	Percentage Fe and Mn mineralization of total
	mmol m^{-1} d^{-1}						%		
Station 23	0.05	0.03	0.03	0.56	1.1	10.0	2.3	11.5	0.3
Station 30	0.02	0.04	0.03	0.05	0.1	2.6	21.9	4.4	1.0
Station 45	0.14	0.12	0.09	0.21	0.5	4.0	18.3	12.8	2.3
Station 53	0.15	0.09	0.08	0.14	0.4	4.5	23.7	7.8	1.8
Station 63	-	0.50	0.25	1.41	3.1	10.7	8.1	26.0	2.3

1086

Biogeosciences Discuss., doi:10.5194/bg-2017-119, 2017
Manuscript under review for journal Biogeosciences
Discussion started: 13 April 2017

Biogeosciences Discussions Open Access EGU

1087

Table 5. Regional estimates of sediment carbon mineralization in the outer Laptev and East Siberian shelf sea

			Dissolved O_2 uptake	Upward DIC flux (anaerobic)	Terrestrial OC-derived DIC flux (anaerobic)	Marine OC-derived DIC flux (anaerobic)	Depth-integrated ^{35}S-SRR (C equivalent)
Outer Laptev Sea	**Average**	**mmol m^{-2} d^{-1}**	4.2	0.16	0.07	0.09	0.09
Outer East Siberian Sea	**Average**	**mmol m^{-2} d^{-1}**	7.2	0.73	0.26	0.47	0.34
Outer Laptev Sea	**280,000 km^2**	**Tg C y^{-1}**	5.2	0.20	0.09	0.11	0.11
Outer East Siberian Sea	**340,000 km^2**	**Tg C y^{-1}**	10.8	1.09	0.39	0.70	0.50
Total outer shelf area	**620,000 km^2**	**Tg C y^{-1}**	15.9	1.28	0.48	0.81	0.62

			^{35}S-SRR-based terrestrial C degradation	^{35}S-SRR-based marine C degradation	Total TEAP-based anaerobic OC degradation rate	Total TEAP-based anaerobic terrestrial OC degradation rate	Total TEAP-based anaerobic marine OC degradation rate
Outer Laptev Sea	**Average**	**mmol m^{-2} d^{-1}**	0.04	0.05	0.15	0.05	0.10
Outer East Siberian Sea	**Average**	**mmol m^{-2} d^{-1}**	0.13	0.21	0.42	0.16	0.26
Outer Laptev Sea	**280,000 km^2**	**Tg C y^{-1}**	0.05	0.07	0.18	0.06	0.12
Outer East Siberian Sea	**340,000 km^2**	**Tg C y^{-1}**	0.20	0.31	0.62	0.23	0.39
Total outer shelf area	**620,000 km^2**	**Tg C y^{-1}**	0.25	0.37	0.80	0.29	0.51

Biogeosciences Discuss., doi:10.5194/bg-2017-119, 2017
Manuscript under review for journal Biogeosciences
Discussion started: 13 April 2017

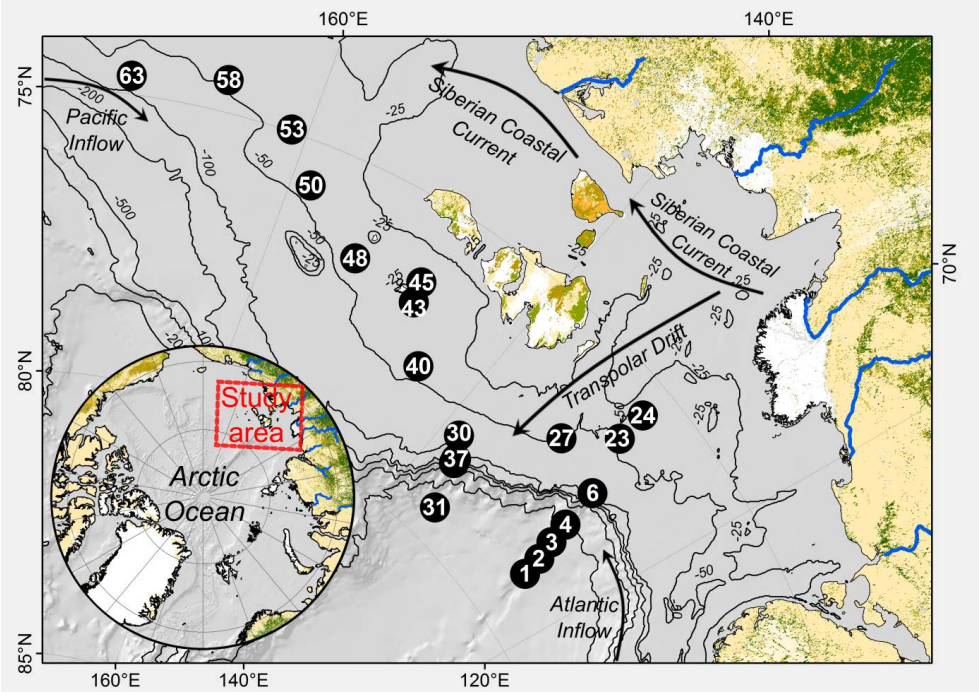

Fig. 1. Map of the Eastern Siberian Sea and slope and station locations.

Biogeosciences Discuss., doi:10.5194/bg-2017-119, 2017
Manuscript under review for journal Biogeosciences
Discussion started: 13 April 2017

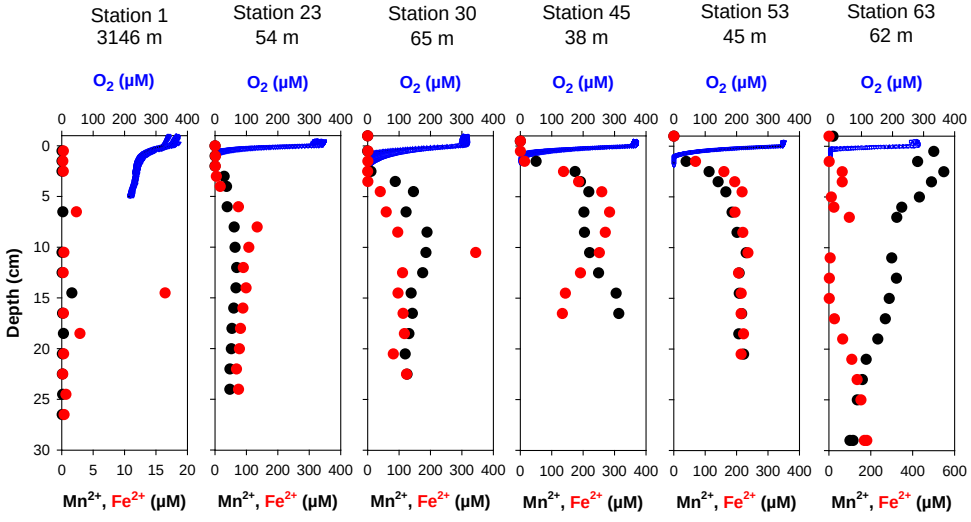

Fig. 2. Depth profiles of dissolved O_2, Fe^{2+}, and Mn^{2+} at Stations 1, 23, 30, 45, 53, and 63. For microelectrode profiles, 4 replicates are shown for each station. Depth resolution of measurement for O_2 was 100 µm.

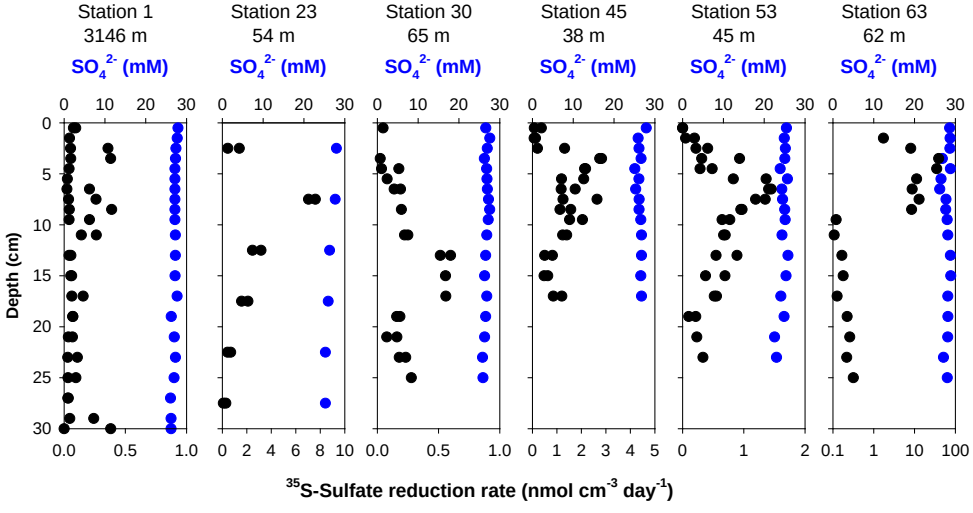

Fig. 3. Depth of profiles of ^{35}S-sulfate reduction rates and porewater concentration of dissolved sulfate for Stations 1, 23, 30, 45, 53, and 63. A replicate incubation was conducted for each depth except for Station 63.

Biogeosciences Discuss., doi:10.5194/bg-2017-119, 2017
Manuscript under review for journal Biogeosciences
Discussion started: 13 April 2017

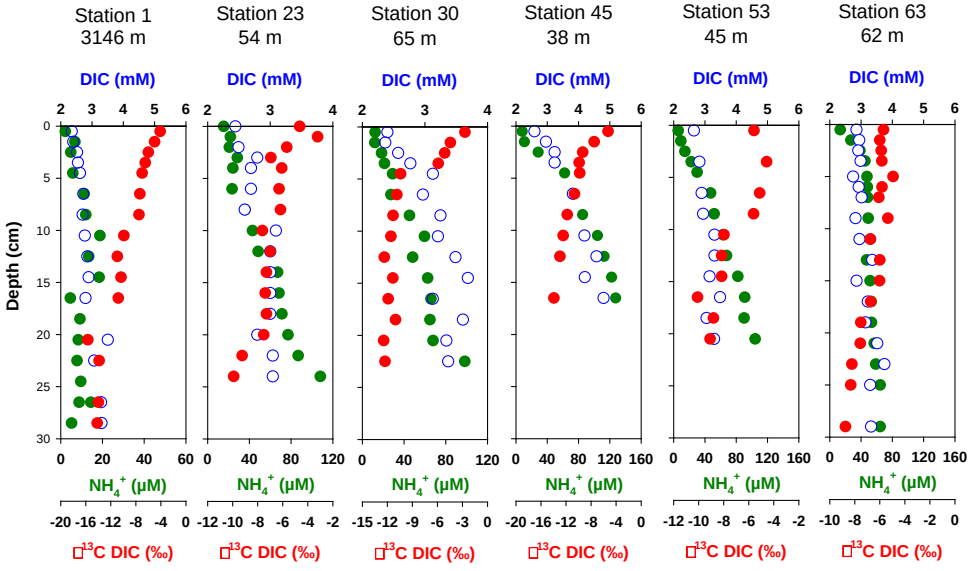

1102

1103 Fig. 4. Depth profiles of porewater dissovled inorganic carbon (DIC), δ^{13}C DIC and porewater NH_4^+ at
1104 stations 1, 23, 30, 45, 53, and 63.

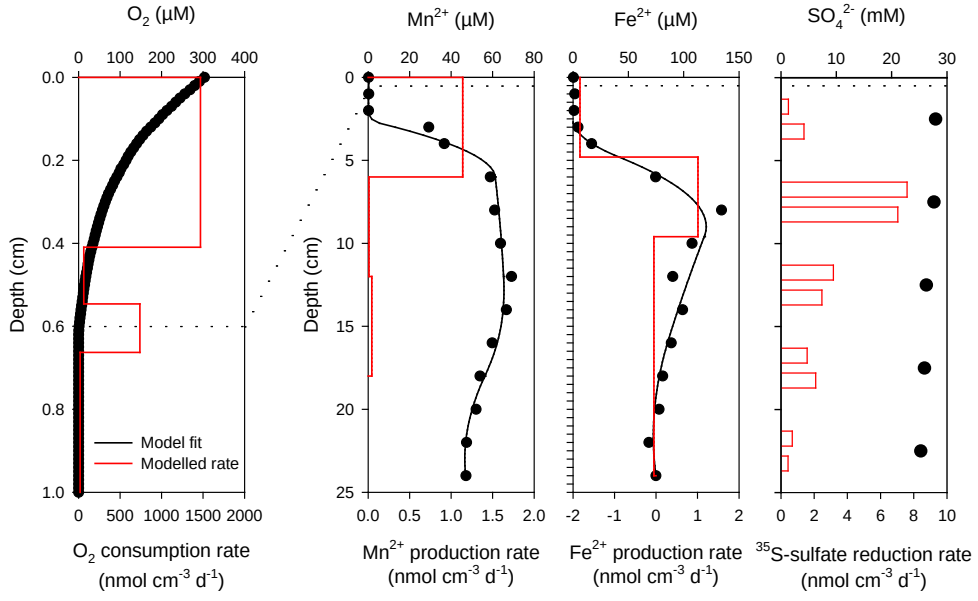

1105

1106 Fig. 5. Comparison of reaction rates of oxygen, manganese, iron, and sulfate reduction at Station 23.
1107 Note the different depth scale for the O_2 consumption rate. The dashed line marks the oxygen
1108 penetration depth.

Biogeosciences Discuss., doi:10.5194/bg-2017-119, 2017
Manuscript under review for journal Biogeosciences
Discussion started: 13 April 2017

1109

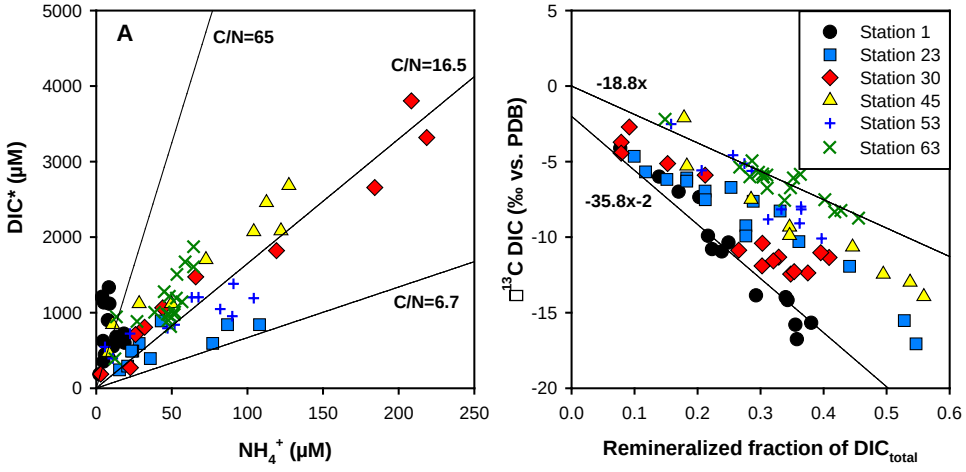

1110

1111 Fig. 6. A: Crossplot of dissolved NH_4^+ and porewater DIC* after correction for bottom water DIC
1112 concentrations. The slopes of the regression lines for the individual stations are shown in Table 2. B:
1113 Crossplot of the fraction of remineralized DIC calculated from a 2-endmember mixing model versus
1114 $\delta^{13}C$ DIC. The slope and y-intercept of the regression for each station are shown in Table 3.

1115

Biogeosciences Discuss., doi:10.5194/bg-2017-119, 2017
Manuscript under review for journal Biogeosciences
Discussion started: 13 April 2017

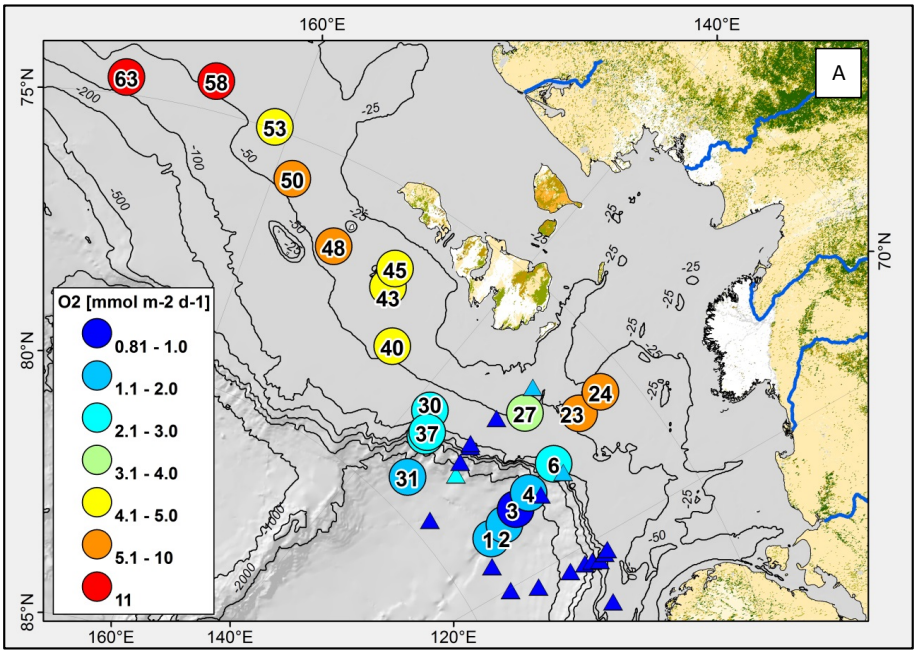

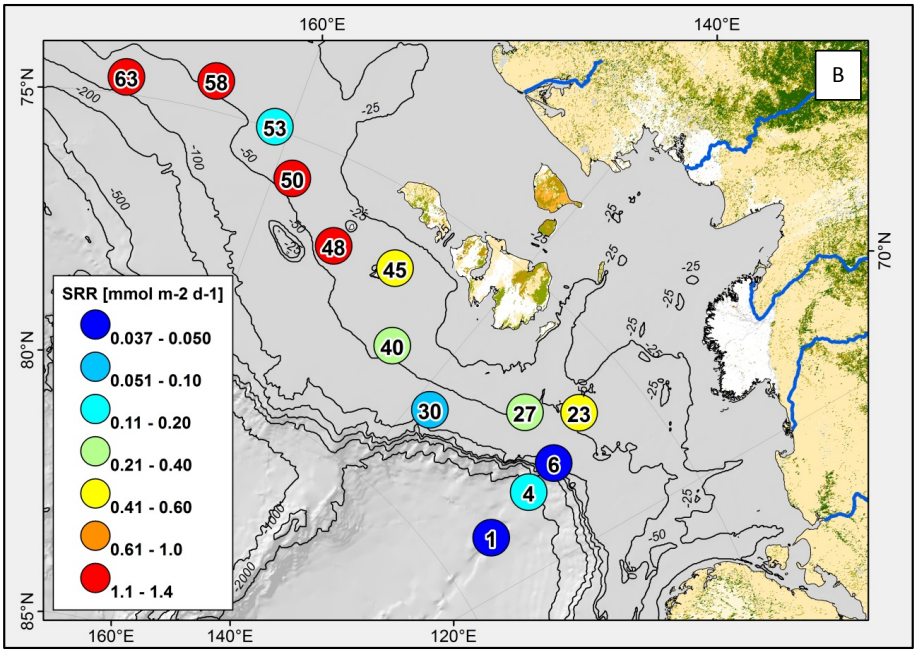

Fig. 7 A, B. Map of field area and sampling stations showing oxygen uptake rates in panel A and depth-integrated sulfate reduction rates in panel B.

Biogeosciences Discuss., doi:10.5194/bg-2017-119, 2017
Manuscript under review for journal Biogeosciences
Discussion started: 13 April 2017

1121

1122

1123

1124

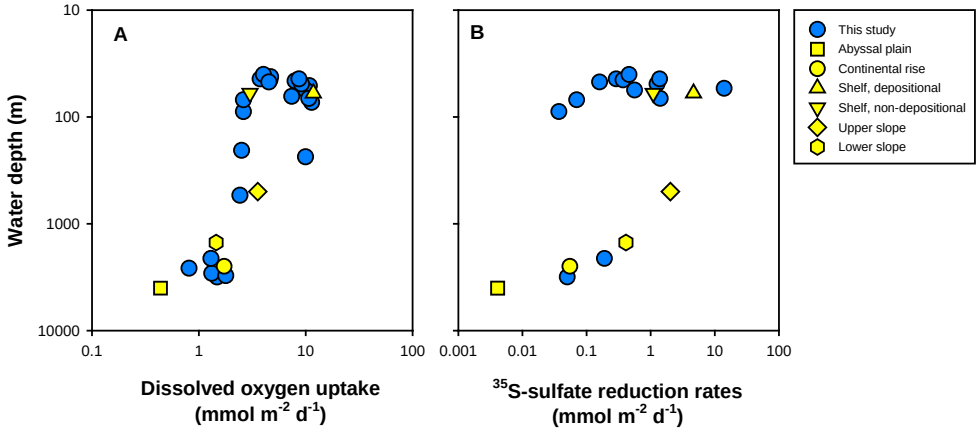

1125

1126 Fig. 8A. Water depth variation of sediment oxygen uptake. 8B: Water depth variation of integrated
1127 ^{35}S-sulfate reduction rates (0-30 cm sediment depth). For reference average rates of abyssal plain,
1128 continental rise, slope, and shelf sediments, deposition and non-depositional, are shown for
1129 reference.

Biogeosciences Discuss., doi:10.5194/bg-2017-119, 2017
Manuscript under review for journal Biogeosciences
Discussion started: 13 April 2017

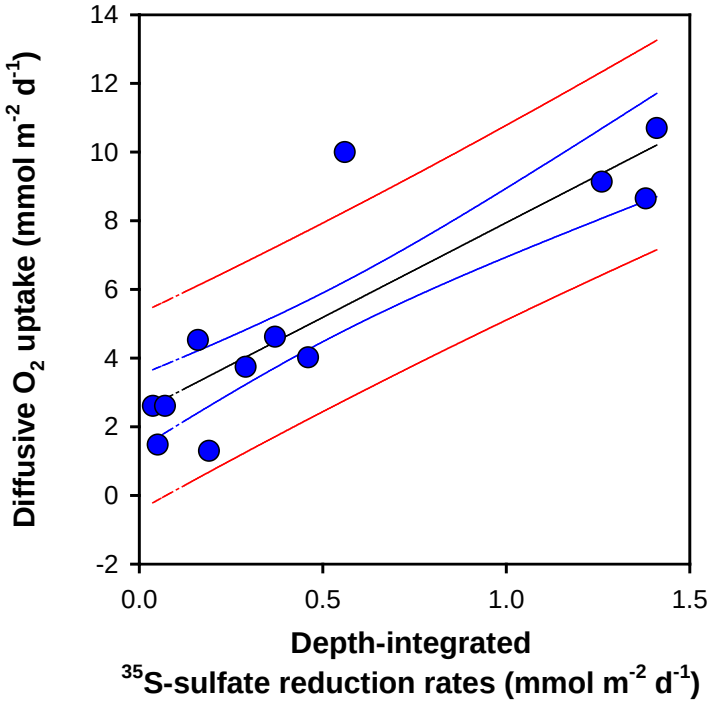

Fig. 9. Crossplot of diffusive oxygen uptake and integrated sulfate reduction rates. The black line is the linear regression and yielded a y-intercept of 2.1 mmol m^{-2} d^{-1} and a slope of 5.55. Blue and red lines show the 95% and 99% confidence interval.